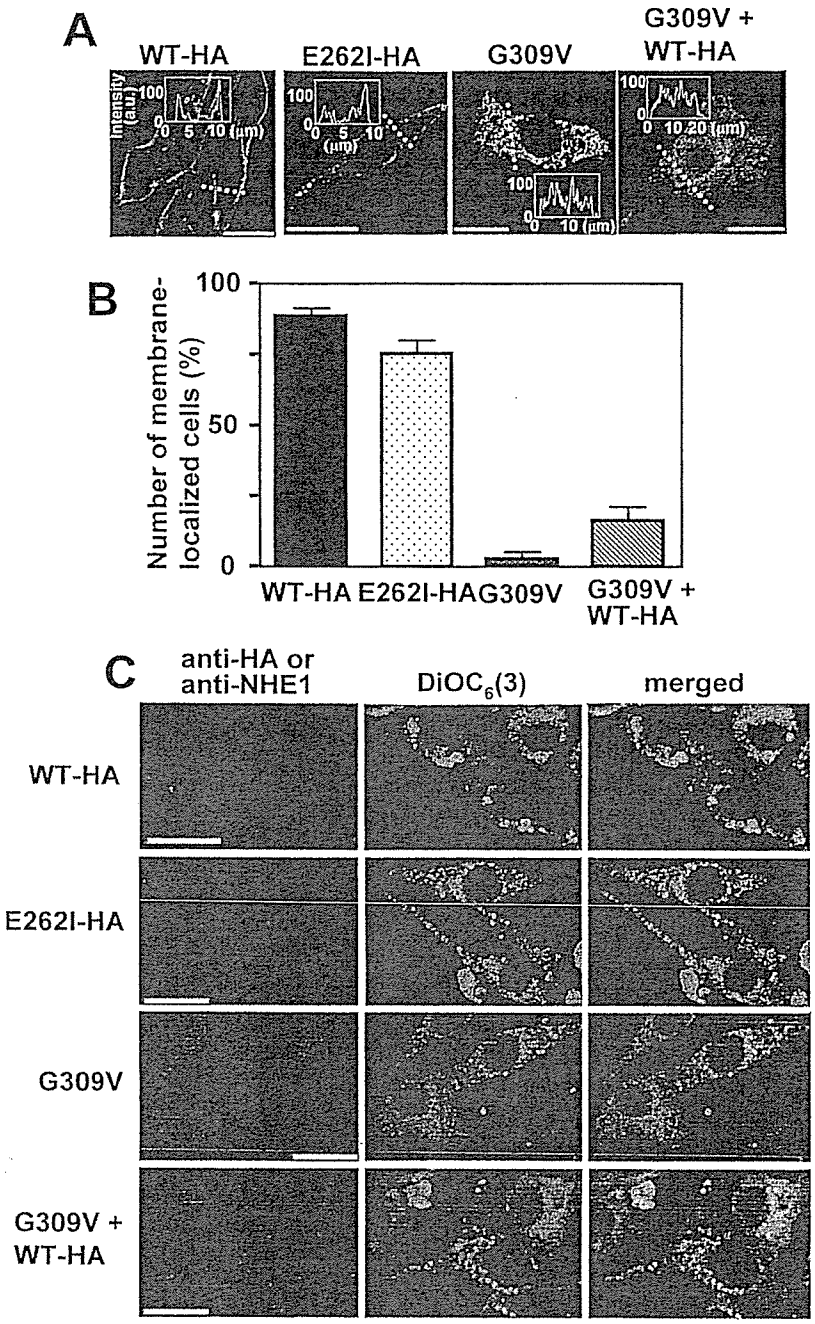

FIGURE 2: Immunofluorescence analysis of two mutant exchangers. (A) Confocal immunofluorescence images of the cells stably expressing the NHE1 variants with or without HA-tag. In one experiment (right panel), cells stably expressing G309V were further transfected with NHE1-HA. Cells were immunostained with anti-HA except for G309V, which were immunostained with anti-NHE1 (third panel). The inset shows the intensity profile of fluorescence along the dotted line. In many cells expressing the wild-type or E262I mutant exchangers, strong fluorescence signals were detected at the cell edge. (B) Summary data for membrane localization of fluorescence signal. The number of cells with a strong fluorescence signal at the cell edge (at least three times more than the average of fluorescence in the internal cell region) was counted. Data are expressed as the mean ± S.D. from six images (total cell number analyzed, 39−101). (C) Double staining of cells for NHE1 and ER maker $DiOC_6$ (*3*). Cells were fixed, permeabilized, and immunostained with anti-HA or anti-NHE1 antibody for G309V (left panels) and then briefly (1 min) incubated with the ER marker $DiOC_6(3)$ (0.1 μM) (middle panels). These fluorescent images were merged (right panels). Scale bars, 20 μm.

G309V and then transfected these cells with HA-tagged wild-type NHE1. In contrast to the predominant localization of the wild-type NHE1 in the plasma membrane upon transfection with a NHE1-carrying vector alone (Figure 2C, left top panel), coexpression of G309V markedly inhibited the surface expression of NHE1 (Figure 2C, left bottom panel and see also Figure 2A and B). Consequently, most of this wild-type NHE1 proteins were retained in the ER, which were co-stained with $DiOC_6(3)$ upon expression of G309V (Figure 2C, right bottom panel). Coexpression also resulted in a strong dominant-negative effect of G309V on exchange activity, as assessed by $^{22}Na^+$ uptake (Figure 1B). Therefore, it is likely that G309V is able to form a heterodimer with the wild-type NHE1 and that dimerization of NHE1 may first occur in the ER membranes, although we do not exclude the possibility that NHE1 subunits interact indirectly.

We next examined whether the wild-type and E262I exchangers exist as a heterodimer in the plasma membrane. We stably coexpressed E262I tagged with an HA epitope (E262I-HA) and the wild-type NHE1 tagged with a Myc

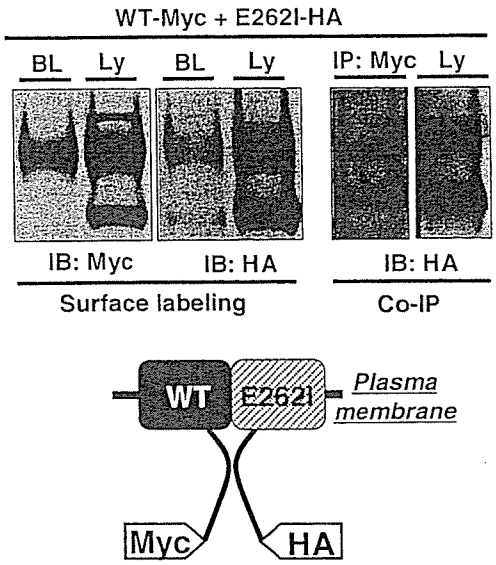

FIGURE 3: Heterodimer formation between the wild-type NHE1 and E262I in the plasma membrane. Cells were stably cotransfected with Myc-tagged NHE1 and HA-tagged E262I and treated with 1 mM NHS-LC-biotin. The biotin-labeled proteins (BL) were collected with streptavidin-agarose beads and analyzed by immunoblotting. Double-transfected cells were also solubilized and subjected to immunoprecipitation with anti-Myc antibody, followed by immunoblotting with anti-HA antibody. The cell lysate was also analyzed by immunoblotting with the indicated antibodies (Ly).

epitope (WT-Myc) in PS120 cells. Cells were surface labeled with NHS-LC-biotin, and biotinylated proteins were recovered with streptavidin-agarose and then analyzed by immunoblotting with anti-HA or anti-Myc antibodies. The results indicate that both proteins were surface-biotinylated (Figure 3), that is, expressed in the plasma membrane. The immature E262I protein band slightly detected in the biotin-treated fraction may be due to the partial membrane permeability of NHS-LC-biotin. To semiquantitatively evaluate the surface expression of NHE1, we estimated the amount of NHE1 proteins adsorbed by streptavidin-agarose beads by subtracting the amount of unbound NHE1 (including immature NHE1) from that of total NHE1 after incubation with beads (data not shown). From such an analysis, we concluded that 45.4 ± 8.7 and 33.3 ± 13.2% (means ± S.D., $n = 3$) of total NHE1 proteins were adsorbed by the beads, that is, expressed in the cell surface for the wild-type and E262I exchangers, respectively. Furthermore, co-immunoprecipitation analysis revealed that E262I-HA was detected in the immunoprecipitates with anti-Myc antibody (Figure 3), suggesting that the Myc-tagged wild-type NHE1 and HA-tagged E262I interact with each other. Hence, surface-labeling and co-immunoprecipitation experiments indicate that wild-type NHE1 forms a heterodimer with E262I in the plasma membrane.

Coexpression of Transport-Deficient NHE1 Mutant Exerts a Dominant-Negative Effect in the Neutral pH_i Range. We next examined the effect of the expression of E262I on the exchange activity of NHE1. We expected that if two active subunits are required for the exchange reaction, heterodimer formation between the wild-type and E262I exchangers would result in the inhibition of activity via the dominant-negative effect of E262I. PS120 cells were transiently transfected with plasmids carrying wild-type NHE1 together with the E262I mutant or an empty vector at a molar ratio of 1:1

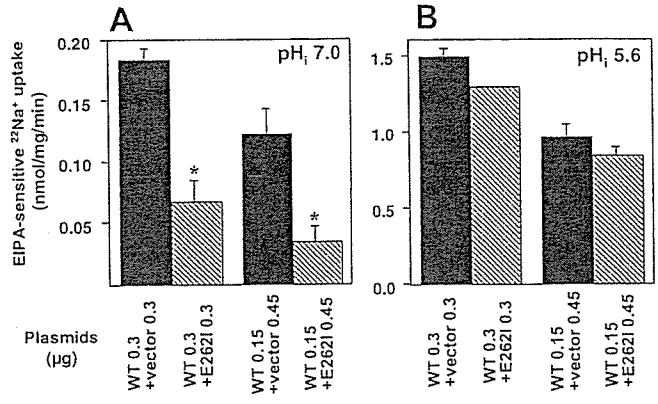

FIGURE 4: Dominant negative effect of E262I on the exchange activity of NHE1. Plasmids carrying the wild-type NHE1 (WT) or E262I were transiently cotransfected into PS120 cells plated on a 24-well plate using Lipofectamine2000. The total quantity of plasmids transfected per well was adjusted to 0.6 μg. In the absence of the E262I plasmid, the total quantity was adjusted with an empty vector. The ratio of the transfected plasmid (WT/E262I or WT/empty vector) was 1:1 and 1:3. Two days after transfection, EIPA-sensitive $^{22}Na^+$ activity was measured at pH_i 7.0 (A) or 5.6 (B) clamped by K^+-nigericin, as described under Experimental Procedures. Values are the means ± S.D. of triplicate determinations. The statistical significance of the data was analyzed by unpaired *t*-test. $^*P < 0.05$.

or 1:3, and exchange activities were assessed by measuring EIPA-sensitive $^{22}Na^+$ uptake at both neutral (7.0) and acidic pH_i (5.6). As shown in Figure 4A, coexpression of E262I resulted in a marked reduction of the activity of the wild-type NHE1 at pH_i 7.0 (more than 50% reduction), that is, E262I exerted the dominant-negative effect. In contrast, expression of E262I had a negligible effect on the exchange activity at acidic pH_i (Figure 4B). These results suggest that heterodimerization with E262I inhibits the transport activity of NHE1 in a pH_i-dependent manner.

We further investigated the dominant-negative effect of E262I under more physiological conditions. To do this, we used CCL39 fibroblastic cells because these cells homogenously express a relatively low amount of endogenous NHE1. The plasmid carrying E262I was cotransfected with DsRed vector carrying a red fluorescent protein as an expression marker. After DsRed fluorescent images were taken, cells were loaded with a fluorescent pH_i indicator, BCECF-AM. Figure 5A shows typical images of DsRed (b) and BCECF fluorescence (c), which were taken in an identical microscopic field. Using this system, the NHE activity was assessed by measuring pH_i recovery after NH_4^+ prepulse. The DsRed-negative cells exhibited a relatively rapid pH_i recovery due to endogenous NHE1 (see cell number 4 in Figure 5A and B). In contrast, the pH_i-recovery rate was dramatically reduced in E262I-expressing DsRed-positive cells (cells numbered 1, 2, and 3). The data from DsRed-positive cells are collected and summarized in Figure 5C and D. While transfection of exogenous wild-type NHE1 accelerated the rate of pH_i recovery, expression of E262I greatly reduced it (Figure 5C and D). Furthermore, expression of E262I shifted the pH_i dependence of the recovery rate to the acidic side (Figure 5E). Figure 5F shows the change in pH_i in response to thrombin. In vector-transfected control CCL39 cells, thrombin induces a rapid cytoplasmic alkalinization via the activation of NHE1, preceded by the transient acidification (asterisk) resulting from Ca^{2+}-

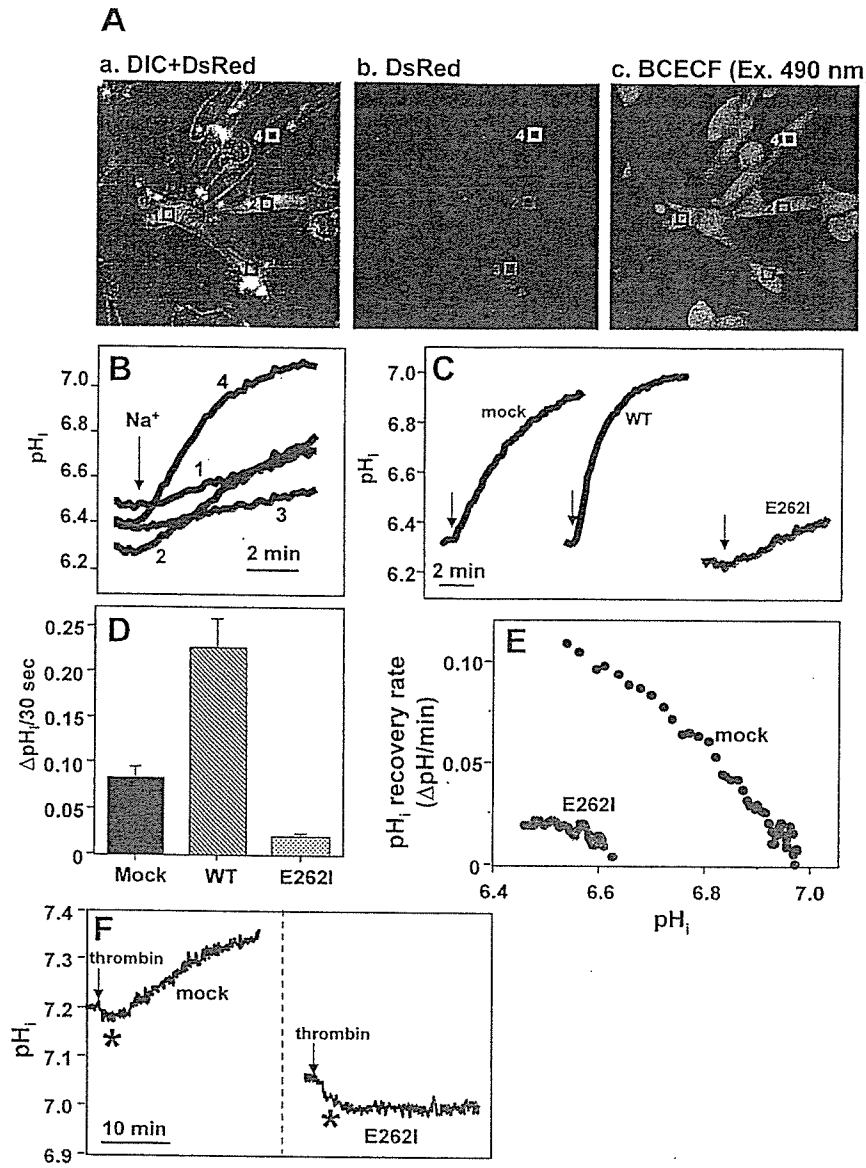

FIGURE 5: Dominant−negative effect of E262I on endogenous NHE1 activity in CCL39 cells. (A) CCL39 cells were grown on collagen-coated glass coverslips and transiently cotransfected with E262I and DsRed (as an expression marker) at a molar ratio of 3:1. Forty-eight hours after transfection, they were serum-depleted for more than 5 h, and a coverslip with a perfusion chamber was mounted on the stage of an inverted microscope fitted with a CCD camera. Differential interference contrast (DIC) and DsRed fluorescence images (a and b) were taken, and then the cells were loaded with 3 μM BCECF-AM for 10 min at room temperature (c, BCECF fluorescence image). (B) pH_i-recovery curves obtained from individually numbered cells. The numbers in B correspond to those in A. Na^+ was added at the time shown by the arrow. (C) and (D) Cells were transiently cotransfected with DsRed together with empty vector (mock), wild-type NHE1, or E262I plasmid, and pH_i-recovery curves were obtained from a DsRed-positive cell. Data were collected from more than 60 DsRed-positive cells in two independent experiments, and a summary of these data is shown. In C, these averaged pH_i-recovery curves are shown, whereas in D, the pH_i increment during 30 s starting from pH_i 6.3 (means ± S.E.) is shown. (E) pH_i dependence of pH_i-recovery rates. The averaged rate of pH_i recovery (C) was calculated from the pH_i increment at every 10 s and plotted against pH_i. (F) Change in pH_i in response to thrombin. CCL39 cells were transiently cotransfected with an empty vector or E262I together with DsRed. At the time indicated by arrows, perfusion was changed to the solution containing 1 uint/mL thrombin. Traces from more than 60 cells were averaged. Asterisks (*) represent the transient acidification resulting from intracellular Ca^{2+} mobilization. These acidifications suggest that cells are capable of undergoing normal cell signaling in response to thrombin.

mobilization (*1*). The expression of E262I completely inhibited this thrombin-induced cytoplasmic alkalinization. Thus, expression of E262I strongly inhibits endogenous NHE1 activity in CCL39 cells in the neutral pH_i range, and thereby abolishes the pH_i regulation in response to growth factors. It should be noted that unlike the $^{22}Na^+$ uptake measurement, we could not assess the exchange activity at very acidic pH_i by measuring pH_i recovery because it was difficult to acidify cells by less than 6.0 by NH_4^+ prepulse.

Na^+/H^+ Exchange Activity Is Inhibited by Symmetrical Intermolecular Cross-Linking at External Cysteine Residues. We expected that if dimerization is essential for the function of NHE1, cross-linking between the two NHE1 subunits would inhibit the Na^+/H^+ exchange reaction by restricting the conformational change of the proteins during transport. We constructed NHE mutants containing a single cysteine using Cys-less NHE1 as a background. Of the 34 single cysteine mutants tested, we found that symmetrical cross-

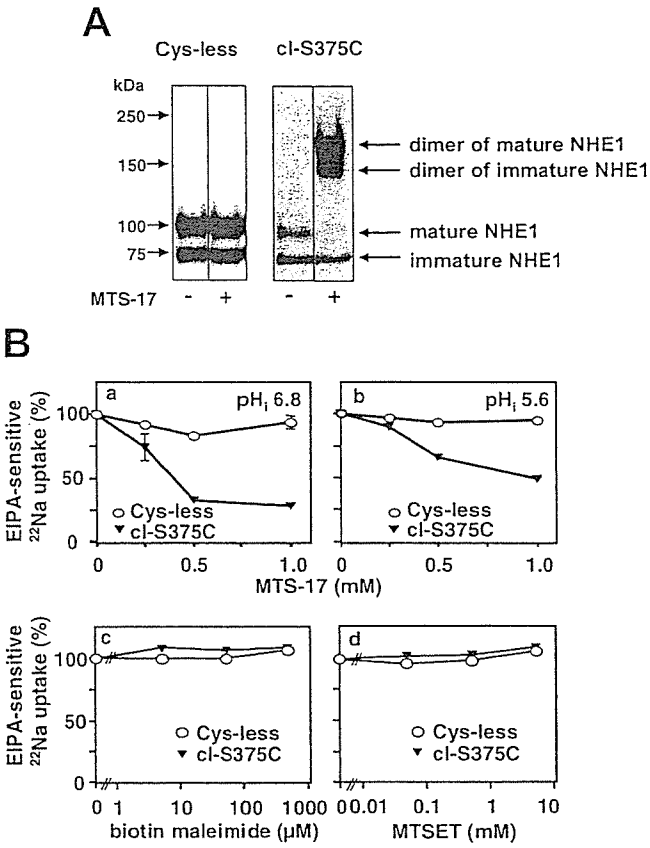

FIGURE 6: Inhibition of NHE1 activity by treatment with cross-linkers. (A) Immunoblot analysis representing the intermolecular cross-linking of cl-S375C proteins. Cells stably expressing Cys-less NHE1 (left panel) or cl-S375C (right panel) were treated with 1 mM MTS-17 for 15 min at 4 °C in BSS and subjected to immunoblot analysis with anti-NHE1 antibody. (B) Cells expressing Cys-less NHE1 or cl-S375C were grown to confluence in 24-well dishes and treated with the indicated concentrations of MTS-17, biotin maleimide, or MTSET for 15 min at room temperature, and the $^{22}Na^+$-uptake activity was measured. In the absence of modifying reagents, EIPA-sensitive $^{22}Na^+$-uptake activity was 10−15 and 40−50 nmol/mg/min at pH$_i$ 6.8 and 5.6 for Cys-less and cl-S375C mutants, respectively. Data were normalized by the values without modifying reagents and represented as means ± S.D. of triplicate determinations. Error bars are sometimes smaller than symbol sizes.

linking occurred with homobifunctional MTS cross-linkers, MTS-2, MTS-6, or MTS-17, at six extracellular sites of NHE1, Pro^{153} in extracellular loop (EL) 2, Asn^{282} and Tyr^{283} in EL4, and Ser^{375}, Thr^{377} and Tyr^{381} in EL5. In this study, we focused on a mutant cl-S375C because a significant reduction of activity was observed upon cross-linking in this mutant. Treatment of the cells with MTS-17 resulted in a mobility shift of cl-S375C from the monomer to the dimer position (right panel of Figure 6A). Immature NHE1 is also cross-linked, as shown by the mobility shift of the lower bands. A similar mobility shift was also observed on treatment with MTS-2 or MTS-6 having shorter spacer arms (data not shown). In contrast to cl-S375C, such a mobility shift was not observed in Cys-less NHE1 (Figure 6A). We investigated whether cross-linking actually affects NHE activity by assessing the effects of cross-linking reagents on EIPA-sensitive $^{22}Na^+$ uptake. Although treatment with MTS-17 had no effect on the activity of Cys-less NHE1, the same treatment markedly suppressed the activity of cl-S375C in a dose-dependent manner both at neutral (6.8) and low pH$_i$ (5.6) (Figure 6B, a and b). Similarly, inhibition of NHE1 activity was also observed as a decrease in the rate of pH$_i$ recovery after acid loading (data not shown). In contrast to MTS-17, the activity was not affected by the monofunctional SH-modifier reagents biotin maleimide or MTSET (Figure 6B, c and d), which have been reported to react with a cysteine residue at position Ser^{375} (*18*), suggesting that inhibition of cl-S375C activity by MTS-17 is not simply due to SH-modification but to intermolecular cross-linking. We did not examine the effects of MTS-2 or MTS-6 on exchange activity because these reagents had a severe toxic effect on cells.

We next investigated several functional properties of cross-linked cl-S375C. As shown in Figure 6B, inhibition of the cl-S375C activity by cross-linking was stronger at high pH$_i$ (75% inhibition at pH$_i$ 6.8) compared to that at low pH$_i$ (50% inhibition at pH$_i$ 5.6). Consistent with this finding, cross-linking with MTS-17 greatly shifted the pH$_i$ dependence of $^{22}Na^+$ uptake to the acidic side and virtually abolished the activity in the neutral pH$_i$ range (Figure 7A), although amino acid substitution of Ser^{375} itself also slightly shifted the pH$_i$ dependence to the acidic side (data not shown). The pH$_i$ dependence of $^{22}Na^+$-uptake activity in Cys-less NHE1 was not affected by treatment with MTS-17 (data not shown). In addition, in cells expressing cl-S375C, cytoplasmic alkalinization in response to thrombin, PMA, or hyperosmotic stress was completely abolished upon treatment with MTS-17 (Figure 7B), whereas significant alkalinization was observed in Cys-less NHE1 (Figure 7B). Lack of NHE1 activation in response to extracellular stimuli is probably due to an acidic shift of the pH$_i$ dependence caused by treatment with MTS-17. In contrast to pH$_i$ regulation, cross-linking with MTS-17 exerted only a small effect on the concentration dependence of extracellular Na^+ (Figure 7C). The K_m values for Na^+ were 8.33 ± 0.64 and 8.95 ± 0.50 mM in Cys-less NHE1 (the trace is not shown) and 12.7 ± 0.7 and 7.99 ± 1.15 mM in cl-S375C in the control and MTS-treated cells, respectively. Treatment with MTS-17 slightly reduced the sensitivity to inhibitor EIPA in cl-S375C (Figure 7D), whereas the same treatment had no effect on EIPA inhibition in Cys-less NHE1 (data not shown). The EIPA concentrations giving half-maximal inhibition (IC_{50}) were 78.23 ± 1.56 and 88.1 ± 11.3 nM in Cys-less NHE1 and 126.0 ± 10.3 and 198 ± 10.6 nM in cl-S375C in control and MTS-treated cells, respectively. These results suggest that cross-linking at extracellular sites has a large influence on exchanger function across the membrane, while exerting a moderate effect on the affinities for extracellular Na^+ and EIPA.

DISCUSSION

In this work, we analyzed the functional significance of the dimerization of NHE1 by means of the expression of a dominant-negative mutant exchanger and intermolecular cross-linking. Initially, we showed that the wild-type NHE1 is capable of interacting with surface expression-deficient G309V and with transport-deficient E262I. These observations, together with the data from cross-linking experiment, reinforce the previous findings that NHE1 exists as a dimer in plasma membranes. Experiments with the dominant-negative mutant NHE1 provided evidence that two active subunits are required for the function of NHE1. The expres-

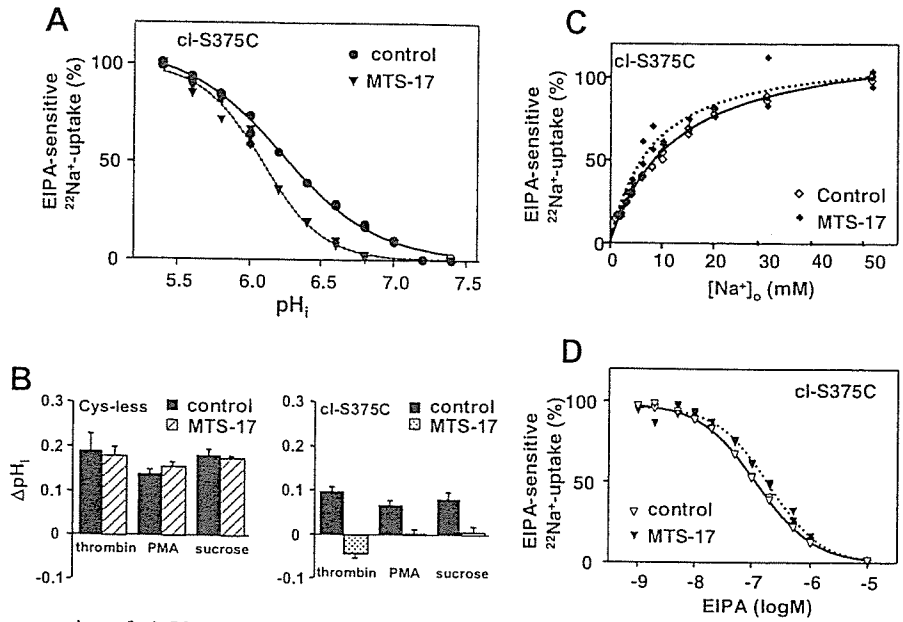

FIGURE 7: Functional properties of cl-S375C after cross-linker treatment. (A) pH_i dependence of EIPA-sensitive $^{22}Na^+$-uptake activity measured in cells expressing cl-S375C treated with or without MTS-17. The $^{22}Na^+$ uptake at pH_i 5.4 was reduced after cross-linker treatment (Figure 6B). Data were normalized to those at pH_i 5.4. (B) Change in pH_i in response to various external stimuli. Cells expressing Cys-less NHE1 or cl-S375C were incubated with or without 250 μM MTS-17 for 15 min at room temperature, and then the external stimuli-induced change in pH_i was measured using the [^{14}C]benzoic acid-equilibration method as described in Experimental Procedures. Cells were stimulated with 1 unit/mL thrombin, 1 μM PMA, or 200 mM sucrose (hyperosmotic stress). (C) and (D) Effect of MTS-17 on the concentration dependences of EIPA-sensitive $^{22}Na^+$ uptake on external Na^+ ($[Na^+]_o$) and EIPA in cells expressing cl-S375C. Cells were treated with 500 μM MTS-17 for 15 min at room temperature and pH_i-clamped at 5.6, and then the $^{22}Na^+$ uptake was measured in the presence of various concentrations of Na^+ (C) or EIPA (D). Data were normalized by the values at 50 mM Na^+ for C or at 1 nM EIPA for D.

sion of transport-deficient E262I in CCL39 cells dramatically reduced the exchange activity of endogenous NHE1 through an acidic shift in the pH_i dependence of exchange activity (Figure 5). In addition, coexpression of E262I, together with wild-type NHE1, markedly reduced exchange activity at neutral pH_i, whereas it exerted only a marginal effect on the activity at acidic pH_i (Figure 4). These data suggest that heterodimer formation between the wild-type protein and the E262I mutant exchanger results in a marked inhibition of exchange activity by inducing an acidic shift of the pH_i dependence, suggesting that dimerization would be essential for physiological exchange activity.

Secondary active transporters such as NHE1 are generally thought to have two major alternating conformations during the transport cycle, outward- and inward-facing orientations. This is also compatible with the recently solved crystal structures of two major facilitator superfamily transporters, the glycerol-3-phosphate transporter (*20*) and the lactose permease of *E. coli* (*21*). In the E262I subunit of the NHE1 heterodimer, such a conformational change may not be able to take place because this subunit is transport-deficient. Therefore, it is possible that the fixed structure of E262I restricts the free motion of a neighboring active subunit. Intermolecular cross-linking would provide another approach to restrict such motion between subunits. The treatment of cells expressing cl-S375C with MTS-17 markedly reduced exchange activity. Importantly, this inhibition mainly occurs by shifting the pH_i dependence of exchange to the acidic side and partly by decreasing the maximal activity at acidic pH_i (V_{max}) and consequently abolished extracellular stimuli-induced cytoplasmic alkalinization. The same treatment, however, did not exert a large influence on the apparent affinities for extracellular Na^+ or the inhibitor EIPA. Intermolecular cross-linking at position Ser^{375}, which is located in EL5, occurred upon treatment with all tested MTS reagents. These reagents have different spacer arms (MTS-2, 5.2 Å; MTS-6, 10.4 Å; and MTS-17, 24.7 Å), suggesting that Ser^{375} in EL5 is mobile over a relatively long distance at least between 5 and 25 Å. In membrane transporters, the movement of extracellular loops often plays an important role in the transport cycle. For example, in the glycine transporter GLYT2, the first extracellular loop is reported to alter its accessibility to SH-modification reagents during the transport cycle (*22*). Our data suggest that cross-linking at position Ser^{375} would restrict the motion of EL5 to less than 25 Å between NHE1 subunits and in turn lead to a marked reduction in exchange activity. These results can be explained if it is assumed that dimerization is essential for NHE1 function and that the two NHE1 subunits undergo conformational changes in a concerted manner. Cross-linking would restrict the coupled motion between the subunits, thereby leading to the inhibition of exchange activity possibly by an apparent reduction in pH_i sensitivity. Thus, the data obtained from two different approaches, the dominant-negative experiment and cross-linking, overall suggest that the exchange activity depends on a coupled conformational change of two subunits at physiological pH_i and raise the interesting possibility that the pH-sensing machinery of NHE1 may be fully functional only when two subunits are active. This idea is consistent with previous reports (*12*–*14*) suggesting that subunit-subunit interaction may be important for the function of the exchanger. For example, the Na^+/H^+ exchange in kidney brush border membrane vesicles was reported to exhibit the sigmoidal Na^+ dependence under certain conditions (*12*, *13*). Also, the pH_i dependence of exchange activity was recently reported to be best explained by allosteric kinetics on the basis of the assumption of a dimeric transporter (*14*).

It is of interest to note that inhibition of activity by expression of E262I was not detected at low pH_i (Figure 4), suggesting that the wild-type NHE1 subunit of the heterodimer is functional when intracellular H^+ concentration is sufficiently high. This is consistent with a previous report demonstrating that the dominant-negative effect of E262I on Na^+/H^+ exchange activity was not detected in measurements taken at acidic pH_i (*9*). This observation may be explained if we assume that E262I affects H^+-regulatory sites but not ion-transport sites of the neighboring active subunit. At present, there is substantial evidence that the ion transport machinery is located within the membrane-spanning region. For example, previous studies have shown that mutations of residues within TM4 and TM9 of NHE1 reduce the affinity for Na^+ or the cation transport activity (*23*−*27*). Furthermore, crystal structure determination and mutational studies on the bacterial Na^+/H^+ antiporter NhaA suggest that the ion binding site consists of several polar residues within the transmembrane helices (*28*, *29*). A high-resolution crystal structure of a bacterial Na^+/Cl^--dependent neurotransmitter transporter homologue provided more direct proof that residues within the transmembrane helices coordinate two Na^+ ions (*30*). Thus, it is reasonable to suppose that each subunit of NHE1 has an ion transport pathway and the active subunit of the heterodimer is capable of catalyzing the transport reaction under particular conditions. However, previous biochemical data (*6*, *8*) suggest that the H^+-regulatory sites and ion-transport sites of exchangers are a part of different structural elements and that the acidic shift in the pH_i dependence of exchange mainly results from decrease in the H^+ affinity at regulatory sites. Recent crystal structure determination of NhaA (*28*) and the subsequent electrostatic analysis (*31*) predicted that charged residues with unusual pK_a values, as the pH-sensor, may undergo protonation/deprotonation reactions and subsequently induce the overall conformational changes resulting in the formation of the active form. In the case of NHE1, we have previously identified crucial elements regulating pH sensing: (i) Arg^{440} in IL5 (*32*), (ii) a juxtamembrane cytoplasmic domain (aa 503−595) (*19*), and (iii) a calcineurin B homologous protein (CHP) interacting with a part of this juxtamembrane domain (*33*, *34*). Arg^{327} in IL4 has also recently been reported to be an important residue for determining H^+ affinity (*14*). Interaction with E262I may possibly modify these regions of the neighboring active subunit. Intermolecular cross-linking at position Ser^{375} may also exert similar effects on H^+-regulatory sites. This led us to predict that these important regions of NHE1 may exist close to the interface between subunits. We recently reported that deletion of the putative juxtamembrane dimer-interface region (aa 560−580) markedly decreased the pH_i-sensitivity of NHE1 (*11*).

The functional significance of oligomerization has only been studied for a few transporters. Some experimental data (*35*−*38*) suggest that NhaA exists as a dimer in membranes and that the subunits may functionally interact. A recent study using a fluorescence resonance energy transfer technique (*38*) suggested that the *Helicobacter pylori* Na^+/H^+ antiporter NhaA monomers exerts conformational change during transport. Furthermore, the transport-deficient mutant form of *Saccaromyces cerevisiae* Na^+/H^+ antiporter Nha1p was reported to exert the dominant-negative effect upon coexpression with the wild-type Nha1p (*39*). These studies suggest the functional importance for dimerization of bacteria and yeast Na^+/H^+ antiporters. The glucose transporter GLUT1 (*40*) and the serotonin transporter SERT (*41*) have also been suggested to function as homo-oligomers, whereas the bacterial lactose permease LacY (*42*) and the renal type IIa Na^+/phosphate cotransporter (*43*) have been shown to function as monomers. However, in the case of NHE1, the functional consequence of dimerization appears to be more complex, that is, dimerization is necessary for NHE1 to function in the physiological pH_i range, although each subunit is capable of functioning at a more acidic pH_i. In this context, it is of interest to note that the lactose transport protein LacS from *Streptococcus thermophilus* was recently shown to be a cooperative dimer in which two subunits are functionally coupled in ΔH^+-driven substrate symport, whereas the monomer is sufficient for substrate/substrate exchange (*44*).

In summary, we presented evidence that dimerization may be essential for NHE1 to exert exchange activity in neutral pH_i range. We predict that two active NHE1 subunits would be required for NHE1 to possess the physiologically relevant H^+ affinity presumably at the H^+-regulatory sites. Although the underlying molecular mechanism is still unknown, our present findings provide good evidence for the functional importance of the dimerization of NHE1.

ACKNOWLEDGMENT

We thank Dr. M. Shigekawa for fruitful discussions and Mrs. M. Nakatani (Ms. M. Ookubo) for technical assistance.

REFERENCES

1. Wakabayashi, S., Shigekawa, M., and Pouyssegur, J. (1997) Molecular physiology of vertebrate Na^+/H^+ exchangers, *Physiol. Rev. 77*, 51−74.
2. Orlowski, J., and Grinstein, S. (2004) Diversity of the mammalian sodium/proton exchanger SLC9 gene family, *Pflugers Arch. 447*, 549−565.
3. Counillon, L., and Pouyssegur, J. (2000) The expanding family of eucaryotic Na^+/H^+ exchangers, *J. Biol. Chem. 275*, 1−4.
4. Putney, L. K., Denker, S. P., and Barber, D. L. (2002) The changing face of the Na^+/H^+ exchanger, NHE1: structure, regulation, and cellular actions, *Annu. Rev. Pharmacol. Toxicol. 42*, 527−552.
5. Slepkov, E., and Fliegel, L. (2002) Structure and function of the NHE1 isoform of the Na^+/H^+ exchanger, *Biochem. Cell Biol. 80*, 499−508.
6. Aronson, P. S., Nee, J., and Suhm, M. A. (1982) Modifier role of internal H^+ in activating the Na^+-H^+ exchanger in renal microvillus membrane vesicles, *Nature 299*, 161−163.
7. Aronson, P. S. (1985) Kinetic properties of the plasma membrane Na^+-H^+ exchanger, *Annu. Rev. Physiol. 47*, 545−560.
8. Wakabayashi, S., Hisamitsu, T., Pang, T., and Shigekawa, M. (2003) Kinetic dissection of two distinct proton binding sites in Na^+/H^+ exchangers by measurement of reverse mode reaction, *J. Biol. Chem. 278*, 43580−43585.
9. Fafournoux, P., Noel, J., and Pouyssegur, J. (1994) Evidence that Na^+/H^+ exchanger isoforms NHE1 and NHE3 exist as stable dimers in membranes with a high degree of specificity for homodimers, *J. Biol. Chem. 269*, 2589−2596.
10. Fliegel, L., Haworth, R. S., and Dyck, J. R. (1993) Characterization of the placental brush border membrane Na^+/H^+ exchanger: identification of thiol-dependent transitions in apparent molecular size, *Biochem. J. 289*, 101−107.
11. Hisamitsu, T., Pang, T., Shigekawa, M., and Wakabayashi, S. (2004) Dimeric interaction between the cytoplasmic domains of the Na^+/H^+ exchanger NHE1 revealed by symmetrical intermolecular cross-linking and selective co-immunoprecipitation, *Biochemistry 43*, 11135−11143.

12. Otsu, K., Kinsella, J., Sacktor, B., and Froehlich, J. P. (1989) Transient state kinetic evidence for an oligomer in the mechanism of Na^+-H^+ exchange, *Proc. Natl. Acad. Sci. U.S.A. 86*, 4818−4822.
13. Otsu, K., Kinsella, J. L., Koh, E., and Froehlich, J. P. (1992) Proton dependence of the partial reactions of the sodium-proton exchanger in renal brush border membranes, *J. Biol. Chem. 267*, 8089−8096.
14. Lacroix, J., Poet, M., Maehrel, C., and Counillon, L. (2004) A mechanism for the activation of the Na/H exchanger NHE-1 by cytoplasmic acidification and mitogens, *EMBO Rep. 5*, 91−96.
15. Bertrand, B., Wakabayashi, S., Ikeda, T., Pouyssegur, J., and Shigekawa, M. (1994) The Na^+/H^+ exchanger isoform 1 (NHE1) is a novel member of the calmodulin-binding proteins. Identification and characterization of calmodulin-binding sites, *J. Biol. Chem. 269*, 13703−13709.
16. Pouyssegur, J., Sardet, C., Franchi, A., L'Allemain, G., and Paris, S. (1984) A specific mutation abolishing Na^+/H^+ antiport activity in hamster fibroblasts precludes growth at neutral and acidic pH, *Proc. Natl. Acad. Sci. U.S.A. 81*, 4833−4837.
17. Wakabayashi, S., Fafournoux, P., Sardet, C., and Pouyssegur, J. (1992) The Na^+/H^+ antiporter cytoplasmic domain mediates growth factor signals and controls "H^+-sensing", *Proc. Natl. Acad. Sci. U.S.A. 89*, 2424−2428.
18. Wakabayashi, S., Pang, T., Su, X., and Shigekawa, M. (2000) A novel topology model of the human Na^+/H^+ exchanger isoform 1, *J. Biol. Chem. 275*, 7942−7949.
19. Ikeda, T., Schmitt, B., Pouyssegur, J., Wakabayashi, S., and Shigekawa, M. (1997) Identification of cytoplasmic subdomains that control pH-sensing of the Na^+/H^+ exchanger (NHE1): pH-maintenance, ATP-sensitive, and flexible loop domains, *J. Biochem. (Tokyo) 121*, 295−303.
20. Huang, Y., Lemieux, M. J., Song, J., Auer, M., and Wang, D. N. (2003) Structure and mechanism of the glycerol-3-phosphate transporter from Escherichia coli, *Science 301*, 616−620.
21. Abramson, J., Smirnova, I., Kasho, V., Verner, G., Kaback, H. R., and Iwata, S. (2003) Structure and mechanism of the lactose permease of Escherichia coli, *Science 301*, 610−615.
22. Lopez-Corcuera, B., Nunez, E., Martinez-Maza, R., Geerlings, A., and Aragon, C. (2001) Substrate-induced conformational changes of extracellular loop 1 in the glycine transporter GLYT2, *J. Biol. Chem. 276*, 43463−43470.
23. Counillon, L., Franchi, A., and Pouyssegur, J. (1993) A point mutation of the Na^+/H^+ exchanger gene (NHE1) and amplification of the mutated allele confer amiloride resistance upon chronic acidosis, *Proc. Natl. Acad. Sci. U.S.A. 90*, 4508−4512.
24. Counillon, L., Noel, J., Reithmeier, R. A., and Pouyssegur, J. (1997) Random mutagenesis reveals a novel site involved in inhibitor interaction within the fourth transmembrane segment of the Na^+/H^+ exchanger-1, *Biochemistry 36*, 2951−2959.
25. Slepkov, E. R., Chow, S., Lemieux, M. J., and Fliegel, L. (2004) Proline residues in transmembrane segment IV are critical for activity, expression and targeting of the Na^+/H^+ exchanger isoform 1, *Biochem. J. 379*, 31−38.
26. Noel, J., Germain, D., and Vadnais, J. (2003) Glutamate 346 of human Na^+-H^+ exchanger NHE1 is crucial for modulating both the affinity for Na^+ and the interaction with amiloride derivatives, *Biochemistry 42*, 15361−15368.
27. Khadilkar, A., Iannuzzi, P., and Orlowski, J. (2001) Identification of sites in the second exomembrane loop and ninth transmembrane helix of the mammalian Na^+/H^+ exchanger important for drug recognition and cation translocation, *J. Biol. Chem. 276*, 43792−43800.
28. Hunte, C., Screpanti, E., Venturi, M., Rimon, A., Padan, E., and Michel, H. (2005) Structure of a Na^+/H^+ antiporter and insights into mechanism of action and regulation by pH, *Nature 435*, 1197−1202.
29. Inoue, H., Noumi, T., Tsuchiya, T., and Kanazawa, H. (1995) Essential aspartic acid residues, Asp-133, Asp-163 and Asp-164, in the transmembrane helices of a Na^+/H^+ antiporter (NhaA) from Escherichia coli, *FEBS Lett. 363*, 264−268.
30. Yamashita, A., Singh, S. K., Kawate, T., Jin, Y., and Gouaux, E. (2005) Crystal structure of a bacterial homologue of Na^+/Cl^--dependent neurotransmitter transporters, *Nature 437*, 215−223.
31. Olkhova, E., Hunte, C., Screpanti, E., Padan, E., and Michel, H. (2006) Multiconformation continuum electrostatics analysis of the NhaA Na^+/H^+ antiporter of Escherichia coli with functional implications, *Proc. Natl. Acad. Sci. U.S.A. 103*, 2629−2634.
32. Wakabayashi, S., Hisamitsu, T., Pang, T., and Shigekawa, M. (2003) Mutations of Arg440 and Gly455/Gly456 oppositely change pH sensing of Na^+/H^+ exchanger 1, *J. Biol. Chem. 278*, 11828−11835.
33. Pang, T., Hisamitsu, T., Mori, H., Shigekawa, M., and Wakabayashi, S. (2004) Role of calcineurin B homologous protein in pH regulation by the Na^+/H^+ exchanger 1: tightly bound Ca^{2+} ions as important structural elements, *Biochemistry 43*, 3628−3636.
34. Pang, T., Su, X., Wakabayashi, S., and Shigekawa, M. (2001) Calcineurin homologous protein as an essential cofactor for Na^+/H^+ exchangers, *J. Biol. Chem. 276*, 17367−17372.
35. Williams, K. A., Geldmacher-Kaufer, U., Padan, E., Schuldiner, S., and Kuhlbrandt, W. (1999) Projection structure of NhaA, a secondary transporter from Escherichia coli, at 4.0 A resolution, *EMBO J. 18*, 3558−3563.
36. Williams, K. A. (2000) Three-dimensional structure of the ion-coupled transport protein NhaA, *Nature 403*, 112−115.
37. Gerchman, Y., Rimon, A., Venturi, M., and Padan, E. (2001) Oligomerization of NhaA, the Na^+/H^+ antiporter of Escherichia coli in the membrane and its functional and structural consequences, *Biochemistry 40*, 3403−3412.
38. Karasawa, A., Tsuboi, Y., Inoue, H., Kinoshita, R., Nakamura, N., and Kanazawa, H. (2005) Detection of oligomerization and conformational changes in the Na^+/H^+ antiporter from Helicobacter pylori by fluorescence resonance energy transfer, *J. Biol. Chem. 280*, 41900−41911.
39. Mitsui, K., Yasui, H., Nakamura, N., and Kanazawa, H. (2005) Oligomerization of the Saccharomyces cerevisiae Na^+/H^+ antiporter Nha1p: implications for its antiporter activity, *Biochim. Biophys. Acta. 1720*, 125−136.
40. Zottola, R. J., Cloherty, E. K., Coderre, P. E., Hansen, A., Hebert, D. N., and Carruthers, A. (1995) Glucose transporter function is controlled by transporter oligomeric structure. A single, intramolecular disulfide promotes GLUT1 tetramerization, *Biochemistry 34*, 9734−9747.
41. Kilic, F., and Rudnick, G. (2000) Oligomerization of serotonin transporter and its functional consequences, *Proc. Natl. Acad. Sci. U.S.A. 97*, 3106−3111.
42. Sahin-Toth, M., Lawrence, M. C., and Kaback, H. R. (1994) Properties of permease dimer, a fusion protein containing two lactose permease molecules from Escherichia coli, *Proc. Natl. Acad. Sci. U.S.A. 91*, 5421−5425.
43. Kohler, K., Forster, I. C., Lambert, G., Biber, J., and Murer, H. (2000) The functional unit of the renal type IIa Na^+/Pi cotransporter is a monomer, *J. Biol. Chem. 275*, 26113−26120.
44. Veenhoff, L. M., Heuberger, E. H., and Poolman, B. (2001) The lactose transport protein is a cooperative dimer with two sugar translocation pathways, *EMBO J. 20*, 3056−3062.

BI0608616

EXPERIMENTAL CELL RESEARCH 312 (2006) 3152–3164

available at www.sciencedirect.com

ScienceDirect

www.elsevier.com/locate/yexcr

Research Article

Identification and characterization of GSRP-56, a novel Golgi-localized spectrin repeat-containing protein

Yuko Kobayashi[a,*], Yuki Katanosaka[a], Yuko Iwata[a], Masayuki Matsuoka[a], Munekazu Shigekawa[b], Shigeo Wakabayashi[a,*]

[a]Department of Molecular Physiology, National Cardiovascular Center Research Institute, Suita, Osaka 565-8565, Japan
[b]Department of Human Life Sciences, Senri Kinran University, Suita, Osaka 565-0873, Japan

ARTICLE INFORMATION

Article Chronology:
Received 30 March 2006
Revised version received
4 June 2006
Accepted 13 June 2006
Available online 27 June 2006

Keywords:
Syne-1
Nesprin-1
Spectrin repeat
Golgi apparatus
Subcellular localization

ABSTRACT

Spectrin repeat (SR)-containing proteins are important for regulation of integrity of biomembranes, not only the plasma membrane but also those of intracellular organelles, such as the Golgi, nucleus, endo/lysosomes, and synaptic vesicles. We identified a novel SR-containing protein, named GSRP-56 (Golgi-localized SR-containing protein-56), by a yeast two-hybrid method, using a member of the transient receptor potential channel family, TRPV2, as bait. GSRP-56 is an isoform derived from a giant SR-containing protein, Syne-1 (synaptic nuclear envelope protein-1, also referred to as Nesprin-1 or Enaptin), predicted to be produced by alternative splicing. Immunological analysis demonstrated that this isoform is a 56-kDa protein, which is localized predominantly in the Golgi apparatus in cardiomyocytes and C2C12 myoblasts/myotubes, and we found that two SR domains were required both for Golgi targeting and for interaction with TRPV2. Interestingly, overexpression of GSRP-56 resulted in a morphological change in the Golgi structure, characterized by its enlargement of cis-Golgi marker antibody-staining area, which would result partly from fragmentation of Golgi membranes. Our findings indicate that GSRP-56 is a novel, particularly small Golgi-localized member of the spectrin family, which possibly play a role in maintenance of the Golgi structure.

Introduction

The structural integrity of biomembranes, including the plasma membrane, Golgi, nuclear, and endosomal membranes, is maintained by a network formed by multiple organellar-specific cytoskeletal proteins. A protein family containing spectrin repeat (SR) motifs, called the spectrin superfamily, is particularly important for regulation of such membrane stability [1,2]. The SR consists of approximately 106 amino acids, with a characteristic triple-helical bundle comprised of three α-helices connected by two loop regions [3,4]. The SR-containing spectrin superfamily proteins, including spectrin, α-actinin, dystrophin, and utrophin, function as the structural support for most cells by forming linkages of membranes with cytoplasmic structures, and also provide the scaffold for a distinct membrane protein complex [1,5]. Spectrin, a conventional SR-containing protein, was first identified as a protein that lines the plasma

* *Corresponding authors.* Y. Kobayashi is to be contacted at the Department of Human Life Sciences, Senri Kinran University, Suita, Osaka 565-0873, Japan. Fax: +81 6 6872 7872. S. Wakabayashi, fax: +81 6 6835 5314.
E-mail addresses: yu-kobayashi@kinran.ac.jp (Y. Kobayashi), wak@ri.ncvc.go.jp (S. Wakabayashi).

0014-4827/$ – see front matter © 2006 Elsevier Inc. All rights reserved.
doi:10.1016/j.yexcr.2006.06.026

membrane. Some spectrin isoforms are also localized to intracellular organelles other than the plasma membrane, such as the Golgi apparatus, endosome/lysosome, and cytoplasmic vesicles [2,6]. For example, it has been reported that at the Golgi apparatus, β-spectrin isoforms form complexes with Golgi-specific ankyrins and cytoskeletal components, and play roles not only in maintenance of Golgi structure but in vesicular transport of membrane proteins [2,7,8].

Recently, a giant SR-containing protein, Syne-1 (synaptic nuclear envelope protein-1, also referred to as Nesprin-1 or Enaptin) was reported. Syne-1 was identified initially as a binding partner for the acetylcholine receptor in skeletal muscle [9] and then shown to be expressed in multiple forms derived from a very large gene (~500 kb) through transcription at alternative initiation sites and mRNA splicing [10,11]. Among these splicing variants, in addition to the putative longest isoform (Syne-1, 1 MDa), Nesprin-1β and Syne-1B are expressed as protein products of 370–380 kDa with broad tissue distribution, while Nesprin-1α, Syne-1A and myne-1 is muscle-specific proteins of 110–130 kDa [9,10,12]. The longest isoform consists of a N-terminal actin binding domain (ABD), a central multiple SR-containing domain and a C-terminal Klarsicht-related (KASH) transmembrane domain that spans the nuclear membrane, has been suggested to play an important role in nuclear positioning [11,13]. The longest isoform has also been suggested to participate in cytokinesis and vesicular transport via the Golgi [14,15]. The smaller Nesprin-1α, which has an SR-domain and a C-terminal domain, has the ability to bind to nuclear protein lamin A/C and emerin, and was suggested to play roles in bridging the nuclear envelope (NE) [12,16]. Moreover, it has recently been demonstrated that Nesprin-1α can bind to muscle A-kinase anchoring protein (mAKAP) and this molecule has been suggested to act as a receptor for mAKAP on NE [17]. These studies raise the interesting possibility that a diverse array of proteins containing different combinations of SR domains derived from the same giant gene may control various cell functions in a tissue-specific and organellar-specific manner. It is likely that there are many other unidentified forms of SR-containing proteins, which may play crucial roles in cellular functions.

In this study, we identified a novel splicing isoform (named GSRP-56) produced from the gene encoding Syne-1 by a yeast two-hybrid method, using a member of the transient receptor potential channel family, TRPV2 (or growth-factor-regulated channel, GRC) as bait. We identified this potential stretch-activated cation channel, TRPV2, previously as a candidate protein responsible for abnormal Ca^{2+} influx in muscular dystrophy and cardiomyopathy [18]. In this study, we showed that GSRP-56 is a novel Golgi-localized isoform of Syne-1 with an apparent molecular mass of 56 kDa, which is different from the splicing isoforms of Syne-1 reported to date. GSRP-56 contains two SR domains, which are necessary for Golgi localization and for interaction with TRPV2. Overexpression of GSRP-56 in HEK cells resulted in enlargement of the Golgi apparatus. Our data indicate that GSRP-56 is a novel spectrin family member possibly regulating the structural organization of the Golgi apparatus.

Materials and methods

Antibodies and other materials

Commercially available primary antibodies were as follows: mouse monoclonal anti-FLAG M2 (Sigma); mouse monoclonal anti-GAPDH (Chemicon); mouse monoclonal anti-GM130 (Golgin-95); mouse monoclonal anti-TGN38; mouse monoclonal anti-nucleoporin-p62; mouse monoclonal anti-adaptin-γ (BD Biosciences). Antiserum against GSRP-56 was obtained by immunizing a rabbit with the GST fusion protein containing the second SR motif of GSRP-56 (aa 259–358). Rabbit polyclonal anti-TRPV2 was reported previously [18]. Brefeldin A, Phusion DNA polymerase, and competent cells (DH5α) were purchased from Sigma, Finnzymes and TaKaRa, respectively. All other chemicals were of the highest purity available. Protein concentration was determined using a Bicinchoninic acid protein assay kit (Pierce) with bovine serum albumin as a standard. RIPA lysis buffer contains 20 mM HEPES, pH 7.4, 150 mM NaCl, 1% deoxycholate, 0.1% SDS, 0.1% Triton X-100, and protease inhibitors.

Yeast two-hybrid screen and isolation of GSRP-56 cDNA

We used MATCHMAKER3 system (BD Clontech) for the yeast two-hybrid screen. A DNA fragment corresponding to the N-terminal cytosolic region (aa 1–167) of mouse TRPV2 fused to the GAL4 DNA binding domain was used as bait and approximately 2×10^7 clones were screened from a human heart cDNA library fused to the GAL4 activation domain (BD Clontech). The screening procedure was essentially as described previously [19]. Colonies that grew in medium lacking histidine, adenine, leucine, and tryptophan (-HALT) were isolated as positive clones and sequenced. From this screen, we sequenced at least 200 positive clones and finally isolated a partial cDNA encoding GSRP-56. This clone was isolated at high frequency (25 colonies, 12% of positive clones sequenced). A full-length cDNA of GSRP-56 was cloned by an additional screen from a human heart large-insert cDNA library (BD Biosciences) using the C-terminal fragment of GSRP-56 as a probe. Library screening was carried out according to the manufacturer's protocol, and the isolated clone was sequenced in its entirety. The genomic sequence was searched using UCSC BLAT search program [20].

For confirmation of the 5′-upstream structure and the entirety of GSRP-56 mRNA, we designed the following primers: F1 (forward), 5′-TTCTGGGTCCTTGTGGCACA-3′; R1 (reverse), 5′-TTTTACATTCGGGCTTTA-3′. Forward and reverse primers correspond to the direct upstream of putative exon 1 and 3′-UTR region of GSRP-56, respectively (black arrows in Fig. 1B). The GSRP-56 cDNA including 5′-upstream region was isolated by the first PCR amplification using these primers and human heart cDNA (BioChain) as the template, and following nested-PCR amplification using the primers adjacent to the first PCR primers (F2, 5′-GACAGGGTCCCCCTGTGTAC-3′; R2, 5′-CGGGCTTTATTTTATTTT-3′. white arrows in Fig. 1B). Protein sequence motifs were detected using the SMART program [21].

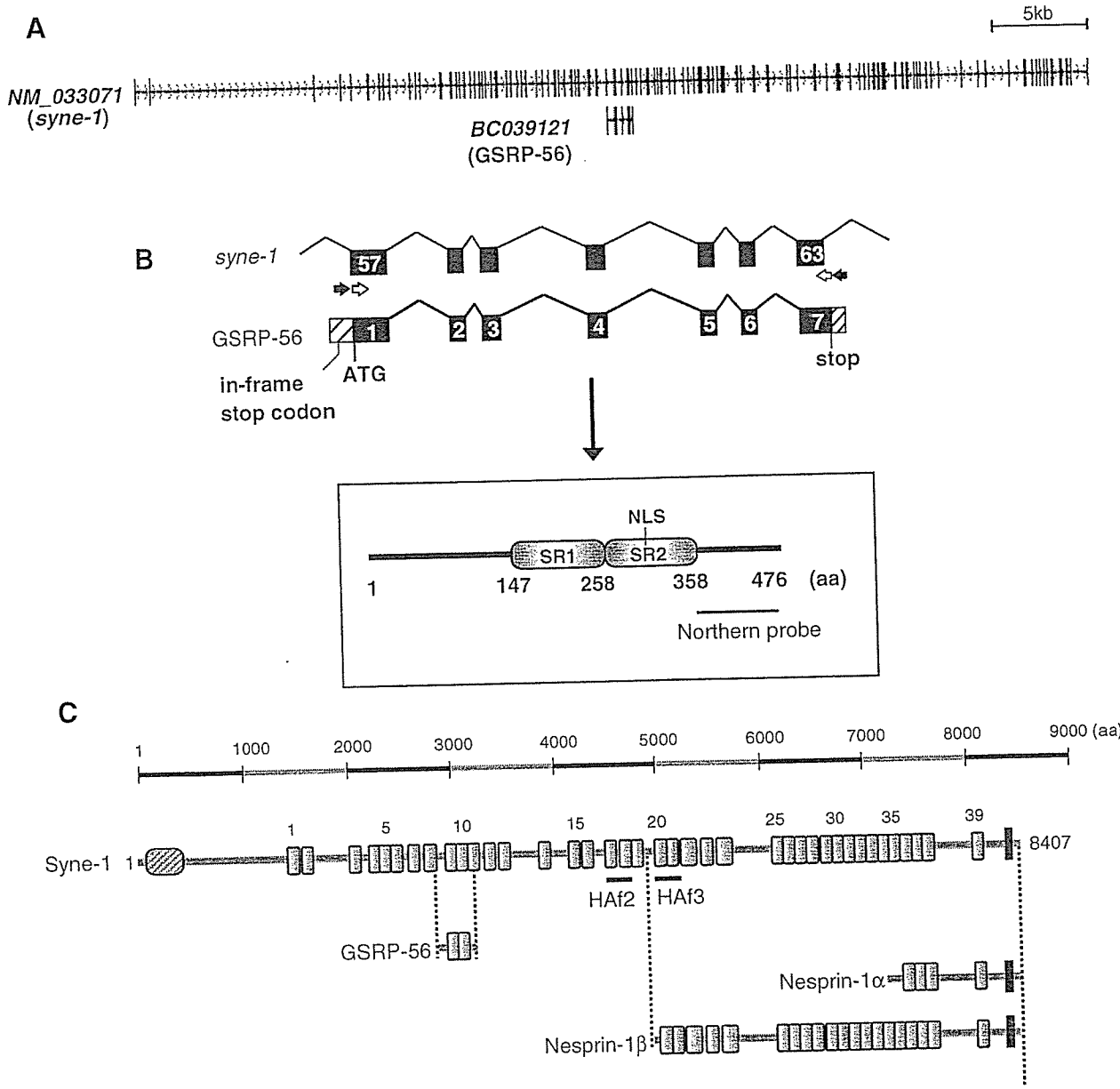

Fig. 1 – Schematic drawing of the gene structure of GSRP-56. (A) Genomic alignment of *syne-1* (GenBank accession no. *NM_033071*) and GSRP-56 (*BC039121*) using the UCSC BLAT program. Vertical lines indicate exons, whereas horizontal lines indicate introns. Small arrows on the vertical lines indicate direction of transcription. (B) Schematic drawings of the gene structures of *syne-1* and GSRP-56. The filled boxes represent exons, and the putative UTR is hatched. GSRP-56 is comprised of 7 exons, and its ORF begins at the position corresponding to exon 57 of *syne-1*. The black and white arrows indicate the region of primers used for PCR amplification of the region 5′-upstream of GSRP-56 (see Materials and methods). The lower panel shows the domain structure of GSRP-56 protein predicted by SMART. Tandem spectrin repeat motifs (SR) are shown. (C) Comparison of the predicted architectures of GSRP-56, longest Syne-1, and its two major splicing isoforms (Nesptin-1α and -1β). The N-terminal actin binding domain (ABD), SR domain, and the C-terminal transmembrane domain are denoted by a hatched box, shaded column, and vertical black bar, respectively. HAf2 and HAf3 represent positions of the proposed Golgi-binding sites of Syne-1 [28].

Northern and PCR analysis

An RNA blot from human multiple tissues (human MTN blot; BD Clontech) was probed with cDNAs labeled with ^{32}P using a random primed DNA labeling kit (Nippon Gene). The cDNA for β-actin (BD Clontech) was used as a positive control. Hybridization was performed at 68°C for 16 h using the ExpressHyb hybridization solution (BD Clontech) and ^{32}P-labeled RNA was visualized using a BAS imaging analyzer (FUJIFILM).

Plasmid construction and purification of recombinant proteins

All of the plasmids used in this study were produced by a PCR-based strategy. For plasmid construction of GST-, FLAG-, or GFP-tagged GSRP-56, PCR fragments corresponding to various regions of GSRP-56 were cloned into pGEX4T-1 expression vector (Amersham Pharmacia), p3xFLAG (Sigma), or pEGFP-C1 (BD Clontech), respectively. After expression of GST fusion proteins in *E. coli*, proteins were purified through glutathione sepharose 4B column (Pharmacia) according to the manufacturer's protocol.

Pull-down assay with GST fusion proteins

Ventricular tissues were taken from rats which were anesthetized according to the Guidelines for Animal Experimentation at the National Cardiovascular Center. Tissues were homogenized in PBS with 1% Triton X-100 by Physcotron (NITI-ON). The lysates were centrifuged and the resultant supernatant incubated with each GST fusion protein together with glutathione beads overnight at 4°C on a rotator. After washing four times with ice-cold PBS containing 0.5% Triton X-100, the bound proteins were eluted with 50 mM Tris–HCl solution containing 40 mM glutathione (pH 8.0) and subjected to SDS-PAGE followed by immunoblotting.

Immunoblotting and immunohistochemistry

Rat tissues and cultured cells were homogenized in RIPA lysis buffer. Extracts were separated on 10% SDS-polyacrylamide gels and transferred onto PVDF membranes (Millipore) as described previously [22]. The blots were visualized using a chemiluminescence detection system (Chemi-Lumi One; Nacalai Tesque) and signals were detected using an ECL-mini camera (Amersham Biosciences). For immunostaining of rat cardiomyocytes and other cultured cells, cells were fixed with 4% paraformaldehyde for 20 min at room temperature before permeabilization. After blocking with Blocking-One reagent (Nacalai Tesque), cells were incubated with primary antibodies diluted with blocking solution as follows: anti-S2, 1:200; anti-GM130, 1:250; anti-TGN38, 1:250; anti-nucleoporin-p62, 1:100; anti-Adaptin γ? 1:500. After washing, cells were incubated with biotin-conjugated goat anti-rabbit IgG secondary antibody (Zymed) diluted 1:500, followed by FITC-Streptavidin complex (Chemicon) diluted 1:1000 or rhodamine-conjugated donkey anti-mouse IgG secondary antibody (Chemicon) diluted 1:500. For antibody preabsorption, anti-S2 (1:100 diluted with PBS) solution was incubated with GST-GSRP-56 fusion protein (aa 1–358) at 4°C, overnight. Usually, aliquots of 10 μg of fusion proteins were added per 100 μl of solution. Fluorescence was observed using a confocal microscope (MRC 1024; Bio-Rad). Measurement of the area stained with anti-GM130 antibody was carried out using image analysis software (NIH Image version 1.63). GFP-negative and -positive cells on the same image were selected and subjected to data analysis.

Cell culture and plasmid transfection

Primary cardiomyocytes were isolated from the ventricles of fetal (embryonic day 21) rats and cultured as described previously [19]. Cardiomyocytes were maintained in M-199 medium (Sigma) supplemented with 10% fetal calf serum (FCS; Gibco) for 4 days before analysis. For immunohistochemical analysis, cells were usually grown on plastic dishes coated with collagen (Cellgen; Koken). C2C12 cells were grown in Dulbecco's modified Eagle's medium (DMEM; Sigma) supplemented with 5% FCS. Cells were grown to confluence, then transferred to differentiation medium containing 2% horse serum, and incubated for 3 days. HEK293 cells were grown in DMEM supplemented with 5% FCS. For transient transfection of plasmids, cells were grown on glass coverslips to 90% confluence and transfected using Lipofectamine 2000 reagent (Invitrogen) in the presence of serum in accordance with the manufacturer's protocol. Usually, 0.6 g of plasmid DNA and 2 μl of Lipofectamine reagent were used for cells on one coverslip. For FLAG-tagged proteins, aliquots of 6 μg of plasmids were transfected into cells in 60-mm dishes using 20 μl of Lipofectamine reagent. Six hours later, transfection medium was removed and cells were cultured with growth medium containing 5% FCS for 24–30 h.

Subcellular fractionation

Subcellular fractionation from rat heart muscles was carried out as described by Kapiloff et al. [23] with slight modifications. A rat heart was disrupted with Physcotron twice at 15,000 rpm for 15 s in 10 ml of Buffer B (10 mM HEPES pH 7.4, 5 mM EDTA, and protease inhibitors) with 0.32 M sucrose. The homogenate was filtered through a cell strainer with pores 100 μm in diameter and subjected to low-speed centrifugation at 3800×*g* for 20 min. The pellet (crude nuclear fraction) was resuspended in 10 ml of buffer B containing 2.4 M sucrose and further centrifuged at 50,000×*g* for 90 min, while the supernatant was centrifuged for 1 h at 100,000×*g*. The resultant pellets (nuclei and crude membrane fractions, respectively) were then resuspended in buffer B containing 0.32 M sucrose and subjected to SDS-PAGE followed by immunoblotting.

Results

Cloning and characterization of GSRP-56 cDNA

To identify the potential regulatory protein of TRPV2, we carried out a yeast two-hybrid screen using the N-terminal cytosolic domain of TRPV2 as bait. One of the positive clones grown on −H/A/L/T high stringency selection plates (see Materials and methods) isolated in the screen was predicted to encode a protein containing multiple SR motifs. By subsequent screening of a human heart cDNA library, we isolated a 1.6-kb cDNA clone that seemed to have the entire open reading frame. Using public EST database information, the sequence of this clone (named GSRP-56, Golgi-localized spectrin repeat-containing protein-56) was shown to be nearly identical to that of an EST clone deposited in GenBank (accession no. BC039121) as 'a partial mRNA of Syne-1' isolated from human testis by the NIH-MGC Project [24]. By genomic sequence search using UCSC BLAT, this clone was predicted to be an as yet unidentified form among

multiple splicing variants produced from the *syne-1* gene (Fig. 1A). The GSRP-56 cDNA is estimated to be produced from seven exons corresponding to exons 57–63 of the large *syne-1* gene with an unspliced intron between exons 63 and 64 (Fig. 1B). This unspliced intron contains a stop codon and subsequent polyadenylation signal sequence. To confirm whether this clone was a partial fragment, we searched for a cDNA clone with a longer 5′-UTR by PCR analysis using primers corresponding to the genomic 5′ upstream sequence and 3′-UTR sequence of GSRP-56, respectively (see Materials and methods). A 1.6 kb cDNA fragment including an in-frame termination codon 146 bases upstream of the first ATG was amplified. Therefore, we concluded that the original cDNA contained the complete ORF. The GSRP-56 cDNA was predicted to encode a protein of 476 aa. Using the SMART algorithm, we found that GSRP-56 contained two tandem SR motifs (Fig. 1B). The second SR contains a nuclear localization signal, although it is unclear whether this motif functions in cells. Fig. 1C shows a schematic drawings of the secondary structures of GSRP-56 and major Syne-1 isoforms reported to date.

Interaction of GSRP-56 with TRPV2

To determine the TRPV2-binding domain of GSRP-56, we purified recombinant GST fusion proteins containing various regions of GSRP-56. Lysate from rat heart was incubated with glutathione beads in the presence of these proteins. After washing and elution with glutathione, we checked the interaction of TRPV2 with these proteins by detecting TRPV2 in the eluted fractions by immunoblotting. We found that endogenous TRPV2 in rat heart bound to GST fusion proteins containing aa 1–358 of GSRP-56 (GST-1–358) as well as full-length GSRP-56 (GST-1–476) (Fig. 2A). TRPV2 also bound to the GSRP-56 protein lacking the second SR domain (aa 1–258), but its binding ability was slightly lower than those of GST-1–358 and GST-1–476. TRPV2 did not interact with GST itself or GST fusion proteins containing aa 1–147 (Fig. 2A). These results demonstrated that two SR domains are required for interaction of GSRP-56 with TRPV2 (Fig. 2B).

Tissue distribution of GSRP-56

Next, we analyzed the tissue distribution of GSRP-56. Northern blotting analysis revealed that the signal for GSRP-56 mRNA (approximately 1.6 kb) was detected predominantly in the human heart, whereas weak signals were detected in skeletal muscle, spleen, kidney, and lung (Fig. 3A). The size of this transcript agreed well with the length of isolated GSRP-56 cDNA. The 1.6-kb transcript seems to be a major product in heart and skeletal muscles, but various other transcripts of different sizes were also detected using our probe on Northern blotting. Subsequently, to evaluate the protein expression of GSRP-56, we prepared rabbit antiserum against the recombinant protein of the second SR region of GSRP-56 (referred to as anti-S2). To evaluate the reactivity of this antiserum, we prepared FLAG-tagged GSRP-56 expressed in HEK293 cells. Immunoblotting analysis demonstrated that anti-S2 strongly recognized the protein

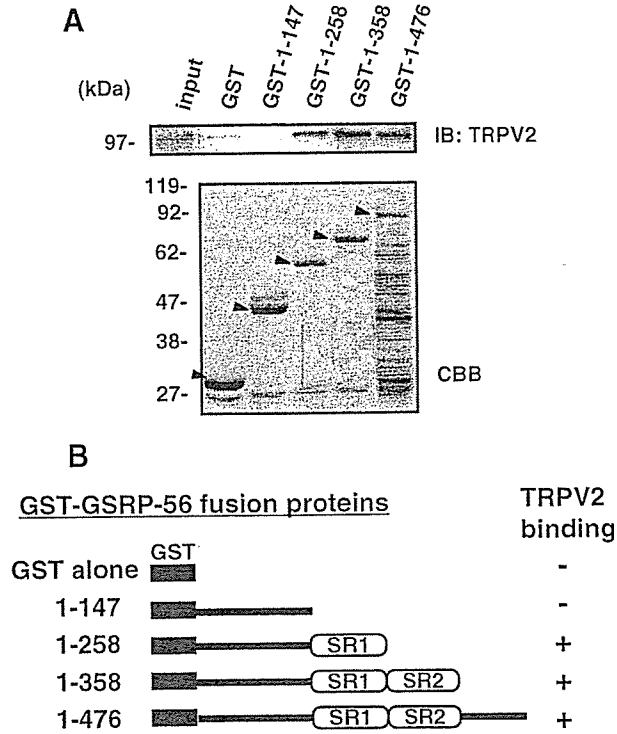

Fig. 2 – Pull-down assay for interaction of GSRP-56 with TRPV2. (A) GST fusion proteins containing various fragments of GSRP-56 were incubated with rat heart homogenate in the presence of glutathione-sepharose beads. After washing, bead-bound proteins were eluted with glutathione as described in Materials and methods. The eluted fractions were detected by immunoblotting analysis with anti-TRPV2 antibody (upper panel). Eluted proteins were stained with Coomassie Brilliant Blue (CBB) to detect the presence of GST fusion proteins (lower panel, arrowheads). (B) Schematic diagram of GST fusion protein constructs containing various regions of GSRP-56 to summarize their binding affinities to TRPV2.

with a molecular mass of 56 kDa, which was the same as that of the protein recognized by anti-FLAG antibody (Fig. 3B). This molecular mass was clearly coincident with that estimated from the primary structure of GSRP-56 (Fig. 3B).

As the 1.6-kb mRNA probably corresponding to GSRP-56 was detected predominantly in heart and skeletal muscles, we examined the protein expression pattern with anti-S2 in these tissues. As shown in Fig. 3C, anti-S2 recognized the 56-kDa protein band in both heart and skeletal muscles, but not in brain. Anti-S2 recognized an additional protein band of ~80 kDa in heart extracts. We considered that this 80-kDa protein band may correspond to another unidentified splicing variant of Syne-1 with the second SR region sequence of GSRP-56. The 56-kDa protein was also detected in the lysate of rat primary cardiomyocytes and mouse C2C12 muscle cells, but not in HEK293 cells with anti-S2 antibody (Fig. 3D). In contrast to the results of immunoblotting analysis of proteins from heart tissues, the 80-kDa band was not detected in cultured cardiomyocytes, although the reason for this observation is not yet clear.

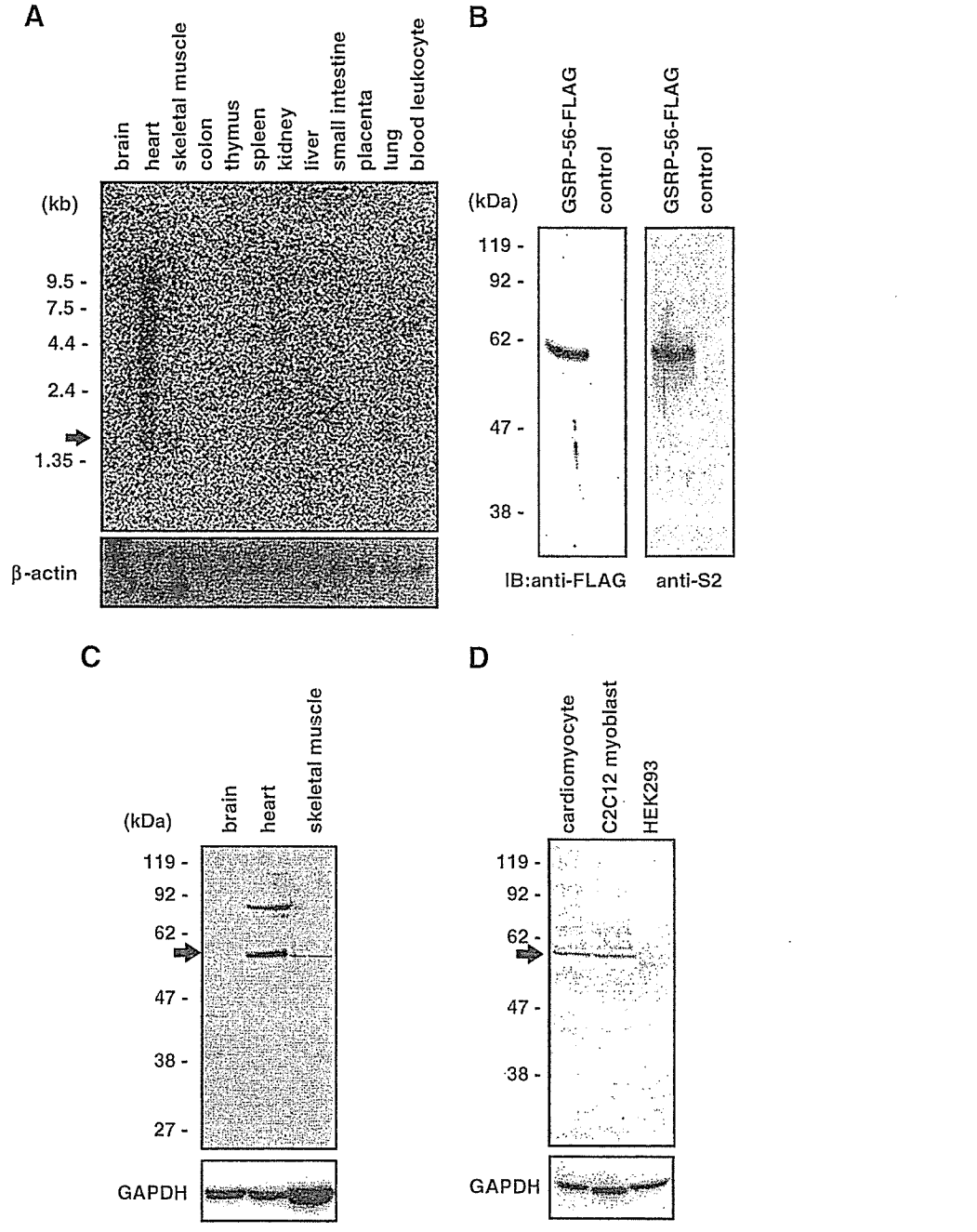

Fig. 3 – Tissue distribution of GSRP-56 transcript. (A) Northern blot of GSRP-56 in adult human tissues. The 1.6-kb GSRP-56 transcript (arrow) was detected predominantly in the heart. The region used as a probe is shown in Fig. 1B. A probe for β-actin was used to ensure equal loading of lanes. (B) Whole-cell extracts from HEK293 cells expressing FLAG-tagged full-length GSRP-56 or no-exogenous protein (control) were analyzed by immunoblotting using anti-FLAG (left panel) and anti-S2 (right panel) antibodies. Anti-FLAG antibody recognized a 56-kDa protein corresponding to the predicted molecular mass of GSRP-56. Anti-S2 antibody was shown to react specifically with the expressed protein. (C) Aliquots of 80 μg of rat tissue proteins were analyzed by immunoblotting with anti-S2 antibody. The antibody recognized 56-kDa protein (arrow). As a control experiment, half the amounts of proteins were analyzed with anti-GAPDH antibody (lower panel). (D) Immunoblotting for proteins from cultured cells. Rat primary cardiomyocytes, mouse C2C12 myoblast cells, and HEK293 cells were cultured and harvested, and homogenized proteins (50 μg) were subjected to immunoblotting analysis with anti-S2 antibody. The antibody recognized 56-kDa protein (arrow). As a control experiment, half the amounts of proteins were analyzed by immunoblotting with anti-GAPDH antibody (lower panel).

Golgi localization of GSRP-56

To analyze the subcellular localization of GSRP-56, we performed immunohistochemical analysis with anti-S2 antibody using rat primary cardiomyocytes and mouse C2C12 muscle cells. Anti-S2 antibody strongly labeled the perinuclear region of rat primary cardiomyocytes (Fig. 4A, a). The Golgi apparatus of cardiomyocytes was reported to be ring-shaped around the nucleus [25]. The staining pattern with antibody against GM130, cis-Golgi matrix protein (Fig. 4A, b) was consistent with these previous reports, and mostly overlapped with the distribution of anti-S2 staining (Fig. 4A, c), suggesting that GSRP-56 is localized predominantly in the Golgi apparatus of cardiomyocytes. As most Syne-1 isoforms have been shown to be localized at the nuclear membrane [9,10,12], which is often located close to the Golgi apparatus, we carried out subcellular fractionation of rat heart tissue to further analyze which organelles are associated with GSRP-56. According to the method described by Kapiloff et al. [23], rat heart homogenate was separated into nuclei and crude membrane fractions. The 56-kDa protein band was enriched in the membrane fraction where TRPV2 and the Golgi marker proteins GM130 and

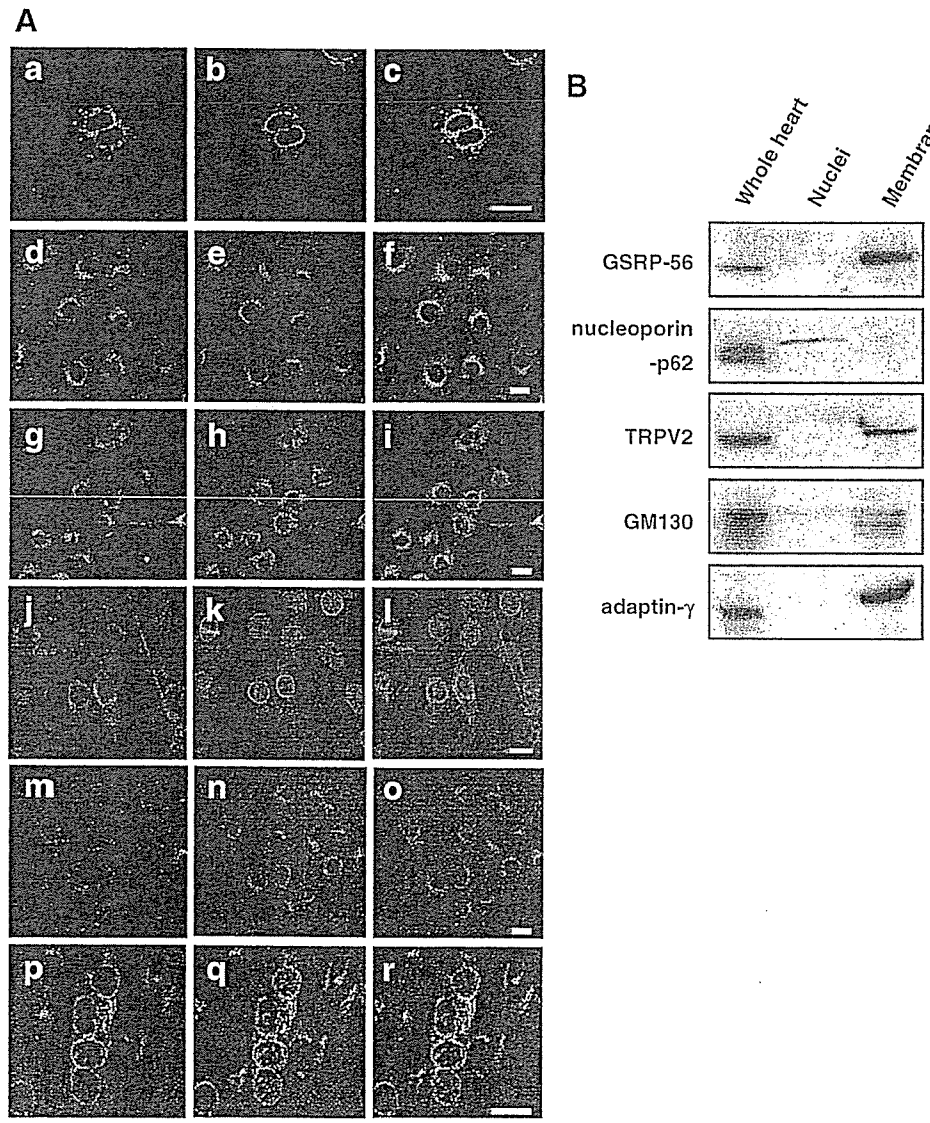

Fig. 4 – Subcellular localization of GSRP-56. (A) Rat primary cardiomyocytes (a–c), C2C12 myoblast cells (d–o), and C2C12 myotubes (3-day culture in differentiation medium, p–r) were double-stained with anti-S2 antibody (a, d, g, j, and p), the antibody for Golgi marker proteins, anti-GM130 (b, e, n, and q) or anti-TGN38 (h), and nuclear marker protein anti-nucleoporin-p62 (k). To test the specificity of antibody, antigen-preabsorbed anti-S2 was used in panel m. Panels c, f, i, l, o, and r show merged images. Scale bar=20 μm. (B) Subcellular fractionation analysis of adult rat heart. Rat heart homogenates were subjected to subcellular fractionation as described in Materials and methods. The crude membrane fraction contained sarcoplasmic reticulum, Golgi apparatus, and plasma membranes. Aliquots of 30 μg of proteins for each fraction were subjected to SDS-PAGE followed by immunoblotting analysis. A 56-kDa protein (GSRP-56) was detected by anti-S2 antibody. Antibodies against nucleoporin-p62 and TRPV2 served as markers for nucleus and membranes, respectively. Antibodies against GM130 and adaptin-γ were used as Golgi markers.

adaptin-γ were detected (Fig. 4B). However, the 56-kDa protein was not detected in nuclei where the nuclear marker nucleoporin-p62 was detected (Fig. 4B). These results suggest that GSRP-56 does not exist in the nucleus.

In C2C12 myoblast cells, anti-S2 antibody labeled distinct perinuclear structures (Fig. 4A, d). This polarized distribution pattern seemed to reflect that of the Golgi apparatus, because this structure was also recognized by the anti-GM130 (Fig. 4A, e). The merged image indicates that the polarized staining patterns with these antibodies overlapped at least partly (Fig. 4A, f). On the other hand, anti-S2 staining did not appear to overlap with that of anti-TGN38, a *trans*-Golgi marker protein (Fig. 4A, g–i) or a nuclear marker protein nucleoporin-p62 (Fig. 4A, j–l). As a negative control experiment, perinuclear labeling was confirmed to disappear when anti-S2 antibody was preabsorbed with the GSRP-56 antigen protein (Fig. 4A, m–o). These results suggest that GSRP-56 is a *cis*-Golgi-localized protein. To evaluate the changes in staining during muscle differentiation, we next performed immunocytochemical analysis in C2C12 myotubes 3 days after switching to differentiation medium (Fig. 4A, p–r). After differentiation, the staining pattern with anti-S2 antibody changed to a more dense ring-shaped distribution around the nucleus (Fig. 4A, p). This ring-shaped structure was well stained with anti-GM130 (Fig. 4A, q) as reported previously in differentiating myotubes [26,27]. These results suggest that GSRP-56 is localized at the Golgi apparatus in both C2C12 myoblasts and differentiated myotubes.

As an alternative approach to evaluate the Golgi localization of GSRP-56, we tested sensitivity to brefeldin A (BFA), a Golgi-destabilizing agent. Previous studies have demonstrated that the Golgi-specific spectrins associate with Golgi membranes in a BFA-sensitive manner [28–30]. Therefore, it was of interest to examine whether BFA treatment would disrupt the association of GSRP-56 with the Golgi complex, as in the case of these proteins. As shown in Fig. 5A, treatment of C2C12 myoblasts for 20 min with BFA resulted in disruption of the stacked Golgi structure as evidenced by staining with anti-adaptin-γ antibody (Fig. 5A, c). The same treatment also induced a rapid dispersion of anti-S2 staining (Fig. 5A, a). A similar effect was observed in C2C12 myotubes (data not shown). We next examined the effects of detergent treatment on GSRP-56 localization. Cells were treated with PBS containing 0.5% Triton X-100 for 10 min prior to fixation leading to the formation of a detergent insoluble structure—a 'Golgi ghost' [28,31]. Previous report have revealed that the Golgi-specific spectrin isoform was retained on tubular vesicular Golgi ghosts even after extraction [31]. The signal detected with anti-S2 antibody disappeared upon detergent treatment (Fig. 5B, a), despite preservation of the Golgi structure as evidenced by staining with anti-GM130 (Fig. 5B, c). These results indicate that GSRP-56 associates with the Golgi apparatus in a BFA-sensitive, but detergent-separable manner.

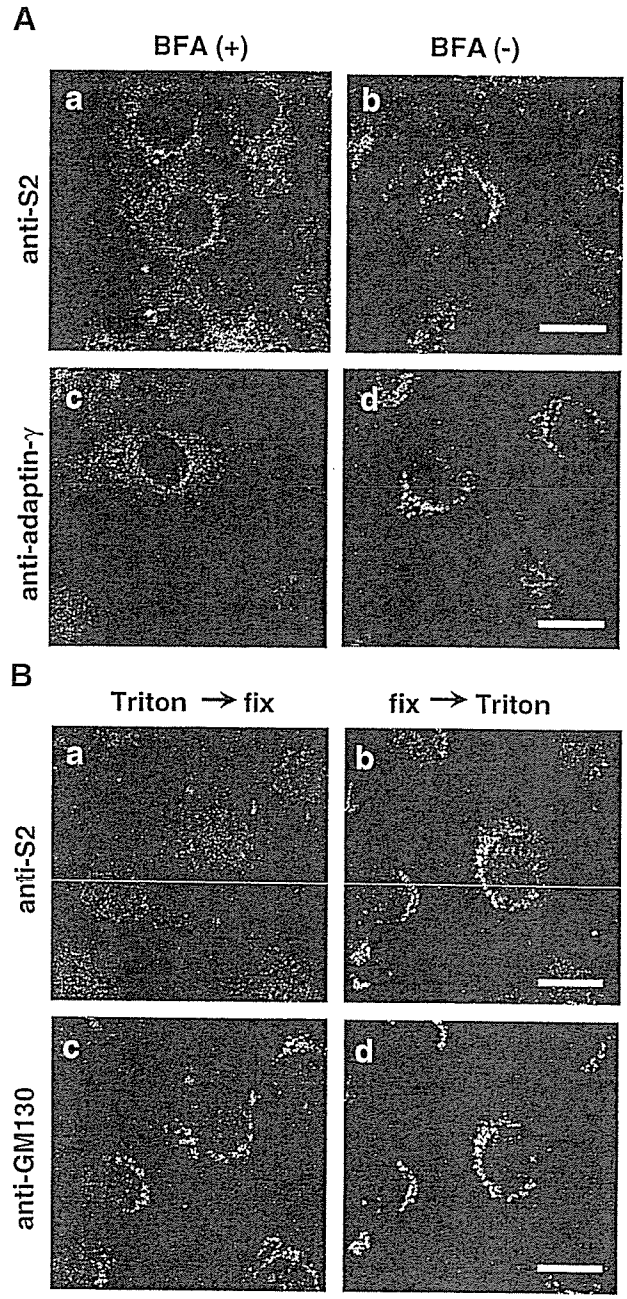

Fig. 5 – Effects of BFA and detergent treatment on Golgi localization of GSRP-56. (A) Effects of BFA. C2C12 myoblasts were treated with (a and c) or without (b and d) 50 μM BFA for 20 min at 37°C before fixation. Fixed cells were stained with anti-S2 antibodies (a and b) or anti-adaptin-γ (c and d). (B) C2C12 myoblasts were treated with 0.5% Triton X-100 for 10 min at room temperature either before (a and c) or after (b and d) fixation. Cells were stained with anti-S2 (a and b) or anti-GM130 antibody (c and d).

Golgi-targeting domain of GSRP-56

To determine the domain(s) that mediate the association of GSRP-56 with the Golgi apparatus, the expression vector carrying GFP-tagged GSRP-56 was transfected into HEK293 cells. The perinuclear concentrated GFP-signal was observed when full-length GSRP-56 (GFP-1–476) was expressed in HEK293 cells (Fig. 6A, a). This polarized localization at least partly overlapped with that of GM130 (Fig. 6A, b and c), further confirming that GFP-1–476 has the ability to target the Golgi in HEK293 cells. Subsequently, GFP-tagged deletion constructs were made and transfected into HEK293 cells. While deletion of the C-terminus (GFP-1–358, Fig. 6A, d–f) did not affect the

Golgi-localization of GSRP-56, deletion of two SR domains (GFP-1–147) completely inhibited the Golgi-localization (Fig. 6A, m, summarized in Fig. 6B). Deletion of the second SR domain (GFP-1–258) preserved the Golgi localization of GSRP-56, although most part of GSRP-56 was distributed in the cytosol (Fig. 6A, g–i). Similar localization patterns were observed in C2C12 myoblasts when GFP-tagged GSRP-56 variants were expressed (data not shown). Notably, a portion of GFP-tagged proteins containing only one or two SR domains were localized to the nucleus (Figs. 6A, j and n), probably due to the nuclear localization signal within the second SR domain. However, GFP-tagged protein with two SR domains (GFP-148–358) retained the ability to associate with the Golgi apparatus (Fig. 6A, j–l). These results suggest that both the first and second SR domains are required for effective targeting of GSRP-56 to the Golgi apparatus.

GSRP-56 changes morphology of the Golgi apparatus

We observed a change in morphology of the Golgi when GFP-tagged full-length GSRP-56 was expressed in HEK293 cells. Interestingly, the clearly enlarged, diffused Golgi structure was observed in GFP-positive cells by immunostaining with anti-GM130 (Fig. 7A, right panel arrowheads) but not GFP-negative non-transfected cells (Fig. 7A arrows). As shown in magnified images (Fig. 7A lower right panel), this enlargement was appeared to be partly derived from fragmentation of Golgi membranes. The area stained with anti-GM130 was measured and summarized in Fig. 7B. Expression of GSRP-56 increased the anti-GM130-stained area by approximately twofold, while expression of the deletion mutant GFP-1–147 lacking the Golgi localization signal had no effect (Fig. 7C, summarized in D), suggesting that GSRP-56 may regulate the morphology of the Golgi apparatus.

Discussion

In this study, we identified a novel SR-containing protein, GSRP-56, as a result of screening for TRPV2-interacting proteins. GSRP-56 is specified as a yet unidentified splicing isoform produced from a giant gene, *syne-1*, in a manner including an unspliced intron insertion. GSRP-56 shows two unique features that have not been reported in other splicing variants derived from *syne-1*. First, the transcript of this isoform is exceptionally small (1.6 kb) and is derived from a central region of the parental gene. Therefore, GSRP-56 protein does not contain any clear functional domains other than two SR domains, although most Syne-1 isoforms have a flanking N-terminal actin binding domain and/or C-terminal transmembrane domain, in addition to multiple SR domains. Thus, GSRP-56 is the rare example having only SR-domains, although CPG2 (candidate plasticity gene 2), a brain-specific Syne-1 isoform that was recently reported to have only SR domains and exert a specific function in the regulation of endocytosis [32], unlike conventional Syne-1 function and localization. Second, GSRP-56 was localized mostly to the Golgi membranes, in sharp contrast to several other splicing isoforms, such as Syne-1A, Nesprin-1α and myne-1, which were reported to be localized to NE [9,10,12]. Recently, Gough et al. [28] isolated a partial fragment of bovine Syne-1 (MDBK clone4) by expression screening performed with Golgi-specific β-spectrin antibody, and reported that Syne-1 is a candidate for Golgi-spectrin [28,33]. Based on the observations that the coding sequence of GSRP-56 does not overlap with that of MDBK clone4 and that GSRP-56 can easily be extracted by Triton X-100 in contrast to detergent-insoluble Golgi-spectrin, we consider that GSRP-56 is a distinct isoform of Golgi-localized Syne-1.

We found that GSRP-56 targets the Golgi apparatus through its tandem SR domains. As GSRP-56 has neither obvious membrane association domains, such as MAD1 and MAD2 of β-spectrins [30,34], nor transmembrane regions, we suppose that its localization is mediated by interactions with other Golgi-localized protein(s). SR-containing proteins including Syne-1 are known to form homo- or hetero-oligomers *via* their SR domains [16,35]. Indeed, by GST pull-down assay we obtained evidence that GSRP-56 interacts with βI-spectrin expressed in heart (data not shown). An A-kinase anchoring protein (mAKAP) has been reported to be targeted to NE via its three SR domains [36], and this targeting was recently reported to occur through the SR-SR interaction between mAKAP and Nesprin-1α in the NE [17]. Therefore, it is likely that GSRP-56 is localized to the Golgi apparatus through SR-mediated interaction with Golgi-specific cytoskeletal proteins. Gough et al. [15,28] proposed two Golgi binding regions of Syne-1, named HAf2 and HAf3. Interestingly, using SMART we found that HAf2 and HAf3 each contain two SRs (see Fig. 1C), similarly to GSRP-56.

In this study, we found that extensive enlargement of the Golgi apparatus occurred in HEK293 cells upon overexpression of GFP-tagged GSRP-56. The observed changes of the Golgi morphology may be caused by derangement of membrane integrity and/or defects in vesicular trafficking systems upon overexpression of GSRP-56. As distinct subtypes of spectrin (βI, βIII) and ankyrin (AnkG119, Ank195) were supposed to form a cytoskeletal meshwork and to function as a structural support of membrane organization [2,8], it is possible that expression of GSRP-56 affects the cytoskeletal organization. Gough et al. [28] reported that expression of the Golgi-binding fragment of Syne-1 (HAf3) in MDBK cells causes compaction of the Golgi apparatus, suggesting that expression of this domain exerts a dominant negative effect by competing with endogenous Syne-1. This apparently opposite effects of two Golgi-targeting polypeptides, GSRP-56 and HAf3, raises the interesting possibility that different SR domains maintain the structure of the

Fig. 6 – Identification of Golgi-targeting domain of GSRP-56. (A) Subcellular localization of GFP-tagged proteins including various regions of GSRP-56 (a–n) and GFP alone (o) in transiently transfected HEK293 cells. Typical expression patterns of each construct are shown. Samples were co-immunostained with anti-GM130 antibody (b, e, h, and k). Merged GFP fluorescence and GM130-stained images are shown in panels c, f, i, and l. Arrowheads and arrows indicate the overlapping or not-overlapping localization of GFP-GSRP-56 and anti-GM130 staining, respectively. Nuclei were labeled by 'N'. Scale bar=20 μm. (B) Schematic representation of GFP-GSRP-56 fusion constructs and summary of the subcellular localization.

A

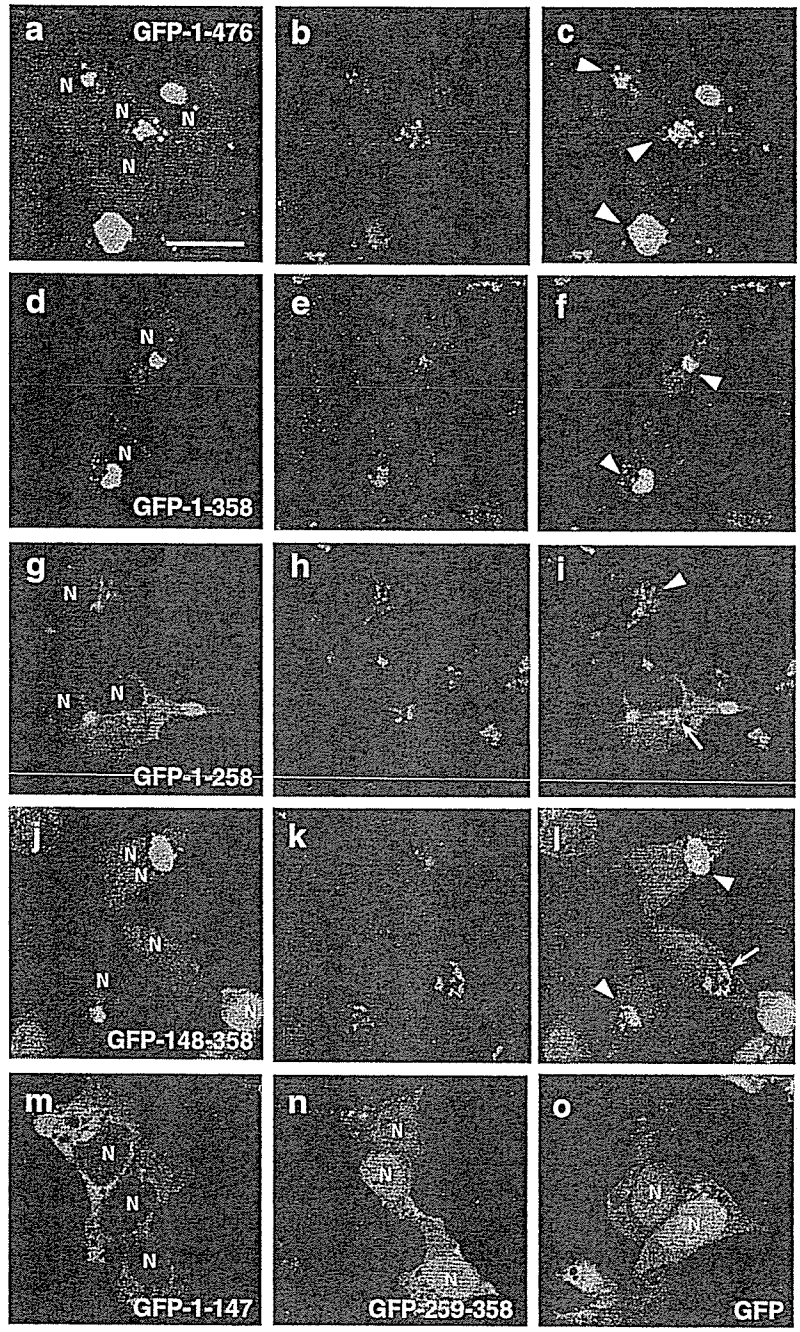
a
GFP-1-476
b
c
d
GFP-1-358
e
f
g
GFP-1-258
h
i
j
GFP-148-358
k
l
m
GFP-1-147
n
GFP-259-358
o
GFP
N

B

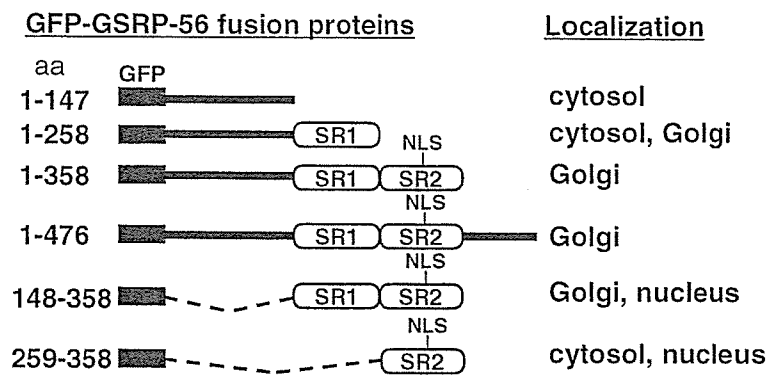
GFP-GSRP-56 fusion proteins
Localization
aa
GFP
1-147
cytosol
1-258
SR1
NLS
cytosol, Golgi
1-358
SR1
SR2
Golgi
NLS
1-476
SR1
SR2
Golgi
NLS
148-358
SR1
SR2
Golgi, nucleus
NLS
259-358
SR2
cytosol, nucleus

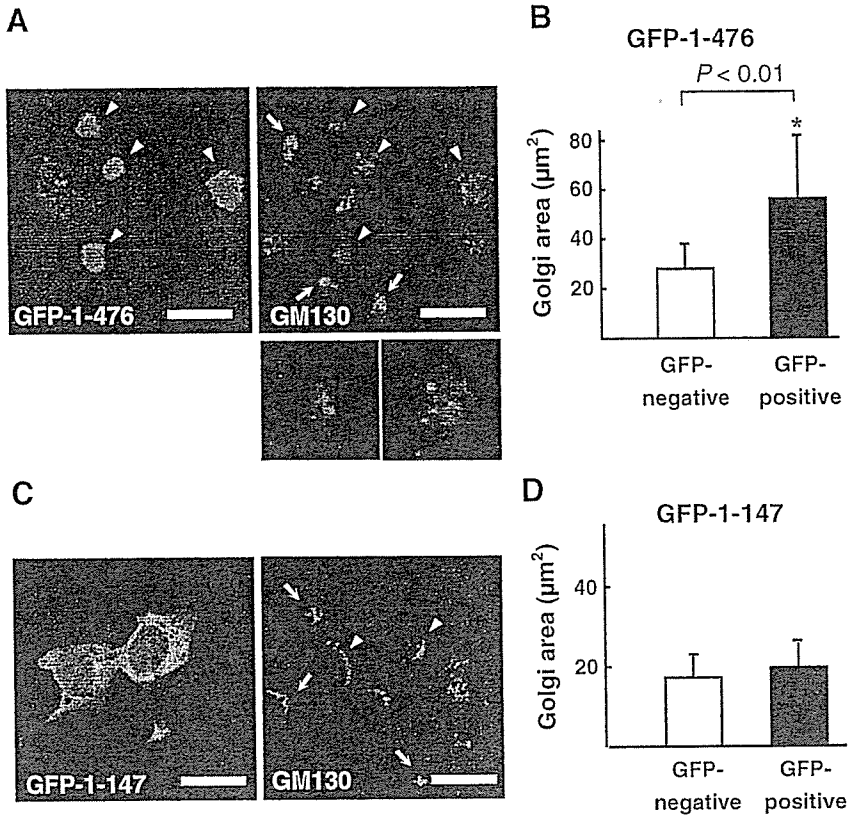

Fig. 7 – Effects of overexpression of GSRP-56 on the morphology of the Golgi apparatus. (A) Images of HEK293 cells transfected with GFP-tagged full-length GSRP-56 (GFP-1–476). GFP fluorescence (left) and staining pattern with anti-GM130 (right) are indicated. GFP-positive and -negative cells are marked by arrowheads and arrows, respectively. The Golgi apparatus of GFP-positive cells appeared to be more enlarged as compared to GFP-negative cells. Scale bar=20 μm. Lower panels show magnified images of typical staining pattern with anti-GM130 of a GFP-negative (left) or a GFP-positive (right) cell. (B) Comparison of anti-GM130 stained areas between GFP-positive and negative cells transfected with the full-length GSRP-56. Data are means±SD of 52 GFP-negative cells (*$P<0.01$ versus GFP-negative cells) and 16 GFP-positive cells, respectively. Mean values were 27.7 μm^2 for GFP-negative cells and 55.2 μm^2 for GFP-positive cells. (C) Images of HEK293 cells transfected with the deletion mutant GSRP-56 (GFP-1–147). GFP-fluorescence (left) and staining pattern with anti-GM130 (right) are indicated. (D) Comparison of GM130-stained areas between GFP-positive and -negative cells transfected with GFP-1–147. Data are means±SD of 20 GFP-negative cells and 17 GFP-positive cells, respectively. Mean values were 17.5 μm^2 for GFP-negative cells and 19.8 μm^2 for GFP-positive cells. The difference in mean value between GFP-negative cells in panels B and D may be due to the differences in experimental conditions of immunostaining.

Golgi apparatus by balancing dilation and compaction under physiological conditions.

Finally, it should be noted that GSRP-56 interacts with the TRPV2 channel. A murine TRPV2 (also referred to as GRC) is known to show regulated translocation from the intracellular compartment to the plasma membrane upon stimulation by growth factors in insulinoma cells [37], by neuropeptide head activator in neuroendocrine cells [38], and by membrane stretching in cultured myotubes [18]. Initially, we isolated GSRP-56 as a candidate for TRPV2 binding protein by a yeast two-hybrid screen. This is the first evidence for a direct interaction of the cytoskeletal element with this channel. However, despite extensive study using cultured cells and tissues, we have not yet confirmed the endogenous interaction between GSRP-56 and TRPV2 by co-immunoprecipitation or immunofluorescence analyses. It is possible that the physiological binding partner for TRPV2 may be the unidentified Syne-1 isoform(s) with larger size, which includes the GSRP-56 sequence. However, we confirmed that GSRP-56 fusion protein certainly had the ability to interact with TRPV2 by GST pull-down analysis. Therefore we suppose that the interaction between these two proteins may be too transient and/or relatively weak to detect *in vivo*. Recently, RGA (recombinase gene activator) was reported to associate with TRPV2 [39]. However, RGA was not co-localized with TRPV2 in the plasma membranes and was suggested to interact with TRPV2 during the biosynthesis and early trafficking of the channel [40]. It is possible that GSRP-56 also exerts such a function as a transient scaffold for TRPV2 or regulates the translocation of TRPV2 through the involvement of other unidentified proteins at the Golgi.

In summary, we identified a novel Golgi-localized isoform of Syne-1, GSRP-56, which is different from the many splicing isoforms of Syne-1 reported to date. We presented evidence that SR domains of GSRP-56 participate in Golgi localization and interaction with TRPV2 and that GSRP-56 possibly play a

role in regulating the membrane morphology of the Golgi apparatus. Clearly, GSRP-56 is a new member with relatively small size among the *syne*-1-derived splicing isoforms, which may exert important physiological functions.

Acknowledgments

This work was supported by the Program for Promotion of Fundamental Studies in Health Sciences of the National Institute of Biomedical Innovation (NIBIO), the Research Grants for Cardiovascular Diseases (17A-1) and for Nervous and Mental Disorders (17B-2) from the Ministry of Health, Labor, and Welfare, a Grant from the Japan Heart Foundation, and Grants-in-aid for Scientific Research on Priority Areas (13142210) and for Exploratory Research (17659241), and a Grant for the Cooperative Link of Unique Science and Technology for Economy Revitalization from Ministry of Education, Science, and Culture of Japan.

REFERENCES

[1] V. Bennett, A.J. Baines, Spectrin and ankyrin-based pathways: metazoan inventions for integrating cells into tissues, Physiol. Rev. 81 (2001) 1353–1392.
[2] M.A. DeMatteis, J.S. Morrow, Spectrin tethers and mesh in the biosynthetic pathway, J. Cell Sci. 113 (Pt 13) (2000) 2331–2343.
[3] J. Pascual, J. Castresana, M. Saraste, Evolution of the spectrin repeat, BioEssays 19 (1997) 811–817.
[4] Y. Yan, E. Winograd, A. Viel, T. Cronin, S.C. Harrison, D. Branton, Crystal structure of the repetitive segments of spectrin, Science 262 (1993) 2027–2030.
[5] K. Djinovic-Carugo, M. Gautel, J. Ylanne, P. Young, The spectrin repeat: a structural platform for cytoskeletal protein assemblies, FEBS Lett. 513 (2002) 119–123.
[6] K.A. Beck, W.J. Nelson, The spectrin-based membrane skeleton as a membrane protein-sorting machine, Am. J. Physiol. 270 (1996) C1263–C1270.
[7] P. Devarajan, P.R. Stabach, A.S. Mann, T. Ardito, M. Kashgarian, J.S. Morrow, Identification of a small cytoplasmic ankyrin (AnkG119) in the kidney and muscle that binds beta I sigma spectrin and associates with the Golgi apparatus, J. Cell Biol. 133 (1996) 819–830.
[8] K.A. Beck, W.J. Nelson, A spectrin membrane skeleton of the Golgi complex, Biochim. Biophys. Acta 1404 (1998) 153–160.
[9] E.D. Apel, R.M. Lewis, R.M. Grady, J.R. Sanes, Syne-1, a dystrophin- and Klarsicht-related protein associated with synaptic nuclei at the neuromuscular junction, J. Biol. Chem. 275 (2000) 31986–31995.
[10] Q. Zhang, J.N. Skepper, F. Yang, J.D. Davies, L. Hegyi, R.G. Roberts, P.L. Weissberg, J.A. Ellis, C.M. Shanahan, Nesprins: a novel family of spectrin-repeat-containing proteins that localize to the nuclear membrane in multiple tissues, J. Cell Sci. 114 (2001) 4485–4498.
[11] V.C. Padmakumar, S. Abraham, S. Braune, A.A. Noegel, B. Tunggal, I. Karakesisoglou, E. Korenbaum, Enaptin, a giant actin-binding protein, is an element of the nuclear membrane and the actin cytoskeleton, Exp. Cell Res. 295 (2004) 330–339.
[12] J.M. Mislow, M.S. Kim, D.B. Davis, E.M. McNally, Myne-1, a spectrin repeat transmembrane protein of the myocyte inner nuclear membrane, interacts with lamin A/C, J. Cell Sci. 115 (2002) 61–70.
[13] R.M. Grady, D.A. Starr, G.L. Ackerman, J.R. Sanes, M. Han, Syne proteins anchor muscle nuclei at the neuromuscular junction, Proc. Natl. Acad. Sci. U. S. A. 102 (2005) 4359–4364.
[14] J. Fan, K.A. Beck, A role for the spectrin superfamily member Syne-1 and kinesin II in cytokinesis, J. Cell Sci. 117 (2004) 619–629.
[15] L.L. Gough, K.A. Beck, The spectrin family member Syne-1 functions in retrograde transport from Golgi to ER, Biochim. Biophys. Acta 1693 (2004) 29–36.
[16] J.M. Mislow, J.M. Holaska, M.S. Kim, K.K. Lee, M. Segura-Totten, K.L. Wilson, E.M. McNally, Nesprin-1alpha self-associates and binds directly to emerin and lamin A in vitro, FEBS Lett. 525 (2002) 135–140.
[17] G.C. Pare, J.L. Easlick, J.M. Mislow, E.M. McNally, M.S. Kapiloff, Nesprin-1alpha contributes to the targeting of mAKAP to the cardiac myocyte nuclear envelope, Exp. Cell Res. 303 (2005) 388–399.
[18] Y. Iwata, Y. Katanosaka, Y. Arai, K. Komamura, K. Miyatake, M. Shigekawa, A novel mechanism of myocyte degeneration involving the Ca^{2+}-permeable growth factor-regulated channel, J. Cell Biol. 161 (2003) 957–967.
[19] Y. Katanosaka, Y. Iwata, Y. Kobayashi, F. Shibasaki, S. Wakabayashi, M. Shigekawa, Calcineurin inhibits Na^+/Ca^{2+} exchange in phenylephrine-treated hypertrophic cardiomyocytes, J. Biol. Chem. 280 (2005) 5764–5772.
[20] W.J. Kent, BLAT-the BLAST-like alignment tool, Genome Res. 12 (2002) 656–664.
[21] J. Schultz, F. Milpetz, P. Bork, C.P. Ponting, SMART, a simple modular architecture research tool: identification of signaling domains, Proc. Natl. Acad Sci. U. S. A. 95 (1998) 5857–5864.
[22] Y. Iwata, H. Nakamura, Y. Mizuno, M. Yoshida, E. Ozawa, M. Shigekawa, Defective association of dystrophin with sarcolemmal glycoproteins in the cardiomyopathic hamster heart, FEBS Lett. 329 (1993) 227–231.
[23] M.S. Kapiloff, N. Jackson, N. Airhart, mAKAP and the ryanodine receptor are part of a multi-component signaling complex on the cardiomyocyte nuclear envelope, J. Cell Sci. 114 (2001) 3167–3176.
[24] R.L. Strausberg, et al., Generation and initial analysis of more than 15,000 full-length human and mouse cDNA sequences, Proc. Natl. Acad Sci. U. S. A. 99 (2002) 16899–16903.
[25] P.J. Kronebusch, S.J. Singer, The microtubule-organizing complex and the Golgi apparatus are co-localized around the entire nuclear envelope of interphase cardiac myocytes J. Cell Sci. 88 (Pt 1) (1987) 25–34.
[26] A.M. Tassin, M. Paintrand, E.G. Berger, M. Bornens, The Golgi apparatus remains associated with microtubule organizing centers during myogenesis, J. Cell Biol. 101 (1985) 630–638.
[27] Z. Lu, D. Joseph, E. Bugnard, K.J. Zaal, E. Ralston, Golgi complex reorganization during muscle differentiation: visualization in living cells and mechanism, Mol. Biol. Cell 12 (2001) 795–808.
[28] L.L. Gough, J. Fan, S. Chu, S. Winnick, K.A. Beck, Golgi localization of Syne-1, Mol. Biol. Cell 14 (2003) 2410–2424.
[29] K.A. Beck, J.A. Buchanan, V. Malhotra, W.J. Nelson, Golgi spectrin: identification of an erythroid beta-spectrin homolog associated with the Golgi complex, J. Cell Biol. 127 (1994) 707–723.
[30] A. Godi, I. Santone, P. Pertile, P. Devarajan, P.R. Stabach, J.S. Morrow, G. DiTullio, R. Polishchuk, T.C. Petrucci, A. Luini, M.A. DeMatteis, ADP ribosylation factor regulates spectrin binding to the Golgi complex, Proc. Natl. Acad Sci. U. S. A. 95 (1998) 8607–8612.
[31] K.A. Beck, J.A. Buchanan, W.J. Nelson, Golgi membrane skeleton: identification, localization and oligomerization of a 195 kDa ankyrin isoform associated with the Golgi complex, J. Cell Sci. 110 (Pt 10) (1997) 1239–1249.

[32] J.R. Cottrell, E. Borok, T.L. Horvath, E. Nedivi, CPG2: a brain- and synapse-specific protein that regulates the endocytosis of glutamate receptors, Neuron 44 (2004) 677–690.
[33] K.A. Beck, Spectrins and the Golgi, Biochim. Biophys. Acta 1744 (2005) 374–382.
[34] C.R. Lombardo, S.A. Weed, S.P. Kennedy, B. Forget, G. Morrow, Beta II-spectrin (fodrin) and beta I epsilon 2-spectrin (muscle) contain NH2- and COOH-terminal membrane association domains (MAD1 and MAD2), J. Biol. Chem. 269 (1994) 29212–29219.
[35] S.P. Kennedy, S.A. Weed, B.G. Forget, J.S. Morrow, A partial structural repeat forms the heterodimer self-association site of all beta-spectrins, J. Biol. Chem. 269 (1994) 11400–11448.
[36] M.S. Kapiloff, R.V. Schillace, A.M. Westphal, J.D. Scott, mAKAP: an A-kinase anchoring protein targeted to the nuclear membrane of differentiated myocytes, J. Cell Sci. 112 (Pt 16) (1999) 2725–2736.
[37] M. Kanzaki, Y.Q. Zhang, H. Mashima, L. Li, H. Shibata, I. Kojima, Translocation of a calcium-permeable cation channel induced by insulin-like growth factor-I, Nat. Cell Biol. 1 (1999) 165–170.
[38] K. Boels, G. Glassmeier, D. Herrmann, I.B. Riedel, W. Hampe, I. Kojima, J.R. Schwarz, H.C. Schaller, The neuropeptide head activator induces activation and translocation of the growth-factor-regulated Ca(2+)-permeable channel GRC, J. Cell Sci. 114 (2001) 3599–3606.
[39] J.C. Barnhill, A.J. Stokes, M. Koblan-Huberson, L.M. Shimoda, A. Muraguchi, C.N. Adra, H. Turner, RGA protein associates with a TRPV ion channel during biosynthesis and trafficking, J. Cell. Biochem. 91 (2004) 808–820.
[40] A.J. Stokes, C. Wakano, K.A. DelCarmen, M. Koblan-Huberson, H. Turner, Formation of a physiological complex between TRPV2 and RGA protein promotes cell surface expression of TRPV2, J. Cell. Biochem. 94 (2005) 669–683.